RHEOLOGICAL AND HEAT TREATMENT ANALYSIS OF SiC/Cf CERAMIC MATRIX COMPOSITES PRODUCED THROUGH DIRECT INK WRITING

by

Trevor Williams

A thesis submitted to the faculty of
The University of North Carolina at Charlotte
in partial fulfillment of the requirements
for the degree of Master of Science in
Mechanical Engineering

Charlotte

2024

Approved By:

_____

Dr. Youxing Chen

_____

Dr. Quiming Wei

_____

Dr. Erina Joyee

ABSTRACT

TREVOR WILLIAMS. Rheological and Heat Treatment Analysis of Sic/Cf Ceramic Matrix Composites Produced Through Direct Ink Writing.
(Under the direction of DR. YOUXING CHEN)

Ceramics and ceramic matrix composites (CMCs) with reinforced fibers have been designed to possess significantly greater fracture toughness and thermal shock resistance. This allows for their potential use in more products such as turbine and combustion engines, hypersonic vehicles, and satellites. Additionally, manufacturing of CMCs allows for the printing of complex geometry for component design pieces. However, currently challenges exist to widespread use. Two major challenges are (a) the fiber alignment that is critical to enhance mechanical properties and (b) the high sintering temperature of ceramics.

In this study, we explored to fabricate Silicon Carbide/ Carbon fibers (SiC/Cf) CMCs by using Direct Ink Writing (DIW) with the purpose of fiber alignment and pyrolysis with the purpose of lowered processing temperature. In addition, this study include ink development through rheological property investigation, as well as pyrolysis parameter optimization (peak temperature and ramping rate) to minimize the thermal cracking and porosity.

This study evaluated the rheological, printing, and pyrolysis properties of ceramic inks to optimize formulations for direct ink writing (DIW) and high-temperature applications. Rheological testing revealed that increasing silicon carbide (SiC) content enhanced shear thinning, with an optimal ratio between 45MK:55SiC and 55MK:45SiC. Fumed silica (FS) also contributed positively to both shear thinning and viscoelastic properties, while carbon fiber (Cf) had minimal impact on shear behavior but was essential for the composite's structural integrity. Printing optimization involved high-speed mixing of MK and IPA for consistency and

constructing a custom syringe extruder to streamline pyrolysis testing, enabling precise extrusion and faster testing cycles. Pyrolysis results showed that fumed silica improved ceramic structure by enhancing matrix bonding, though higher processing temperatures were sometimes necessary for complete ceramic formation. Ink B, exhibiting shear thickening, failed during DIW, suggesting that shear properties are more crucial than the presence of a crossover point. Lack of carbon fibers in the final products indicated oxidation during pyrolysis, highlighting a need for an inert environment to preserve fiber integrity. Comparisons of various inks confirmed fumed silica's role in reducing cracking and increasing stability, while optimal SiC content was identified for stable ceramic structures. Future research will focus on minimizing thermal stress and cracking by testing in inert environments, potentially with argon, to mitigate carbon oxidation. Additional studies will also explore the effects of carbon fiber alignment, distribution, and bonding with the matrix to improve toughness in high-temperature ceramics. These findings provide foundational insights for enhancing DIW-compatible ceramic formulations and guiding future material design for improved performance in extreme conditions.

ACKNOWLEDGEMENTS

I would like to express my deepest gratitude to my advisor, Dr. Youxing Chen, for his invaluable guidance, encouragement, and support throughout the course of this research. His expertise and patience have been instrumental in the completion of this work. I am also immensely grateful to my thesis committee members, Dr. Erina Joyee and Dr. Quiming Wei, for their insightful feedback and advice which have greatly improved the quality of this thesis. A special thank you to Dr. Erina Joyee and Anasheh Khecho for granting me access to the rheology lab and equipment which was essential for conducting key experiments in this research. Your assistance and generosity are greatly appreciated. I wish to also express my gratitude for Dr. Jeff Raquet for assisting in the 3D printing for our project. I would also like to extend my sincere thanks to Tien Herd for her help and guidance with the use of the furnace for pyrolysis. The support made a significant impact on the successful completion of this project. Finally, I would like to thank all my colleagues, friends, and family who have supported me throughout this journey.

TABLE OF CONTENTS

LIST OF TABLES

LIST OF FIGURES

LIST OF ABBRIVIATIONS

CMC	Ceramic Matric Composite
CES	Cambridge Engineering Selector
AM	Additive Manufacturing
LCMC	Lightweight Ceramic Matrix Composites
DIW	Direct Ink Writing
PSMQ	Preceramic Polymer Poly (methyl-silsesquioxane)
TGA	Thermogravimetric Analysis
SEM	Scanning Electron Microscope
FEG	Field Energy Guns
TEM	Transmission Electron Microscopy
SE	Secondary Electrons
BSE	Back scattered electrons
IPA	Isopropyl Alcohol

CHAPTER 1: INTRODUCTION

1.1 Ceramic Composite Composites

Ceramics are a strong material and therefore could be useful in the development of many products. Product potentials range from turbines in energy applications to space vessels in the aerospace field. Yet while ceramics are praised for their high strength and toughness in the presence of high temperatures, they contain a major flaw that prohibits their use in many applications. Traditional ceramics are extremely brittle. This trait often leads to sudden and catastrophic failure of component parts made from ceramics resulting in damage to the entire system the piece interacts with. One of the largest issues is the low fracture toughness that ceramics show which leads to brittle failure with no plastic deformation being present before the failure [1]. The problem therefore is how to achieve the manufacturing of a part with the desired mechanical properties of a ceramic while improving the fracture toughness. A potential solution to this problem is the manufacturing of Ceramic Matrix Composites (CMCs) for use in product piece development instead of pure ceramics.

1.1.1 Ceramic Composite Material Selection

Ceramic Matrix Composites, commonly referred to as CMCs, are advanced materials that combine the high-temperature capabilities and stiffness of ceramics with the strength and toughness of composite materials [2]. They consist of ceramic fibers or whiskers embedded in a ceramic matrix [3]. The composite design is facilitated for engineers through the use of databases which allow for the rapid selection of the optimal material by considering various factors such as material properties, cost, and process requirements. These databases, such as the Cambridge

Engineering Selector (CES), provide engineers and designers with powerful tools to efficiently identify and compare materials. These tools help ensure that the chosen material meets the specific criteria for performance, budget, and manufacturing processes [4]. When complex requirements need to be met, various material properties that contribute to the same requirement can be combined to create a material index. And while these indices help in evaluating the suitability of different materials for specific applications, different requirements can sometimes lead to conflicting objectives. To manage these conflicts, trade-off surfaces are constructed in the material index charts. These charts provide a visual representation of how different materials perform against multiple criteria, allowing for a balanced selection based on the prioritized needs of the project [5].

CMCs are designed to overcome the brittleness of monolithic ceramics, with the matrix failing first under load [6]. CMCs are tough and can withstand high temperatures and corrosive atmospheres, making them suitable for thermos-structural applications [6]. These materials are also known as inverse composites, meaning that the failure strain of the matrix is lower than that of the fibers. This is the opposite of what is observed in most polymer or metal matrix composites, where the fibers typically fail before the matrix. Consequently, in inverse composites, the matrix is the first to fail under load. To prevent the brittle fibers from failing prematurely when the matrix begins to microcrack, it is crucial to control the fiber-matrix (FM) bonding during the processing stage. This careful control ensures that the fibers can sustain the load even after the matrix starts to degrade, thereby enhancing the overall durability and performance of the composite [6].

1.1.2 Composite Material in the Current State of Use

Two broad categories of CMCs are CMCS with (a) continuous fibers and (b) chopped/milled fibers. Generally, these fibers are made from ceramic materials, such as SiC, carbon, and oxides. These materials can withstand high temperatures required for the composite processing and arrest cracks through deflection at fiber/matrix interfaces [7]. Continuous fiber-reinforced CMCs are a promising material for high-tech applications due to their specific properties, including high-temperature strength, chemical inertness, and irradiation tolerance. Among these composites, continuous fiber-reinforced silicon carbide CMCs (CMC-SiC) have been extensively researched and developed [8] for high-tech fields like aeronautics and astronautics. In parallel, a range of chopped and milled fibers have also been explored for use in CMCs with a focus on enhancing mechanical properties, especially fracture toughness [9]. These fibers can also be made from a variety of materials, with specific properties and applications [10]. For example, Al_2O_3 chopped fibers have been used to improve the mechanical properties of Ti_2AlC composites, making them potential high-temperature structural materials [11].

Continuous fibers provide numerous advantages when used in ceramic matrix composites such as improved strength, stiffness, fracture toughness, and fatigue resistance. [7, 12, 13] The strength and stiffness of the continuous fibers are better than those of the chopped/milled fibers because they enable load transfer/distribution. These continuous fibers also improve the fracture toughness by increasing the crack deflection. Crack deflection is a property typically seen in composite materials where the propagating crack hits a different phase or reinforcement causing the cracks movement to be changed or impeded. This increase in crack deflection is an optimal property as it stops cracks from propagating as quickly. In addition, the energy required for the crack to overcome the phase or reinforcement will be much greater. This serves to further stop

cracks from propagating along the part. However, challenges remain in their development and implementation. One of the biggest drawbacks is the manufacturing/implementation costs and impact damages they can sustain. The increase in cost is due to the complexity involved in implementation of these continuous fibers into the matrix resulting in an anisotropic structure. This structure means that these CMCs cannot be used in applications where the stresses/forces are multidirectional. Lastly, CMCs that typically use continuous fibers are highly susceptible to impact damage leading to delamination and/or fiber breakage. Ongoing research focuses on toughening mechanisms, fabrication processes, interfacial characteristics, and interface modification to further enhance CMC performance [12]. Many of the disadvantages discussed above can be fully or at least partially solved by using the second form of composite materials typically seen in CMCs, milled/chopped fibers.

Milled or chopped fibers have the length at the micro and sometimes nanoscale. These fibers, when used in a CMC, have the potential to increase the ease of manufacturability, turn the CMC more isotropic, decrease the cost involved in their production, and increase the damage tolerance. Chopped fiber reinforcement can enhance mechanical properties, such as flexural strength and fracture toughness, while offering cost-effective production compared to continuous fiber reinforcement [11-14]. These fibers offer another layer of complexity as according to Pienti *et al.* the way these milled/chopped fibers are prepared can also lead to a change in their performance and/or role within the CMC [15]. The chopped fibers also come with some disadvantages. CMCs that use chopped fibers typically experience lesser mechanical properties, such as fracture toughness, strength, and stiffness, compared to those made with continuous fibers. The way that the fibers align could also be an issue. Depending on how they are oriented in the CMC, it could

change the properties of the CMC. Lastly using chopped/milled fibers could limit the CMC's use in higher temperature applications.

1.1.3 Ceramic Matrix Composites Production

CMCs are an often-complex composite that combine multiple types of ceramics, composites, and additives to form a single cohesive part. Due to the high complexity involved in their manufacturing there are many ways of producing these CMCs. There are typically two broad categories of production methods. Traditional manufacturing methods and the additive manufacturing (AM) methods. Traditional manufacturing methods are a set of established and conventional methods used to transform raw materials into finished products through various processes. Additive manufacturing is commonly referred to as 3D printing. It is a process to create three dimensional objects, based off a digital model, by adding material(s) in a layer-by-layer fashion until the part has been completely constructed.

1.1.4 Traditional Manufacturing Methods

Various production methods have been developed for CMCs, including infiltration techniques like polymer infiltration and pyrolysis, chemical vapor infiltration, reactive melt infiltration, hot pressing, hot isostatic pressing, spark plasma sintering, and powder metallurgy [16-18]. Traditional methods are well-established processes resulting in methods that have been extensively studied and optimized. This work has resulted in better mechanical properties in the outcome with the parts typically having a higher density and minimal defects. Traditional methods, while expensive, are more cost effective for large-scale manufacturing operations. Techniques like chemical vapor infiltration (CVI) and polymer infiltration and pyrolysis (PIP)

can produce materials with complex chemistries and microstructures that are challenging to achieve with AM. However, these methods do contain some disadvantages, CMCs produced through traditional methods are more complex and costlier to produce. These methods also impose geometric constraints because these methods usually require multiple steps, molds, or dies to manufacture. These parts also result in large lead times and numerous production cycles being required leading to a significant increase in the time required to make the finished product.

1.1.5 Additive Manufacturing Methods

Recent research on CMCs focuses on advancing manufacturing techniques to overcome traditional challenges. Additive manufacturing (AM) has emerged as a promising approach. AM enables the production of damage-tolerant ceramic composites with co-continuous phase reinforcement inspired by natural materials. Various AM techniques have been successfully applied to CMC fabrication, including stereolithography, powder-based methods, selective laser melting, direct ink writing, binder jetting, fused deposition modeling, and many more methods [19-21]. AM's biggest advantage over traditional manufacturing is the ability to produce parts with complex or customized geometries. AM also allows parts to be created without the need for molds or long development cycles. These methods also allow for less waste to be created as it only deposits what is needed on each layer. These parts are also useful because it becomes possible with the increase in complexity to add multiple functions into a single part thus improving its overall performance even more. However, challenges remain with producing parts through AM. One major challenge is achieving optimal mechanical properties and geometric accuracies. The number of materials that can be used is limited compared to the materials that can be used in traditional manufacturing. AM parts will typically have a lower surface quality

and resolution resulting in geometrical inaccuracies. Lastly, while AM parts are easy to produce for custom, on demand pieces. it is not the best for large-scale production.

1.1.6 The Future of CMC Design and Production

Ongoing research focuses on improving the properties of CMCs, such as wear resistance, thermal stability, and self-healing capabilities. These improvements would enhance their performance in various application fields, including nuclear energy parts, turbine parts, and cutting tool designs [17]. Additionally, researchers are exploring other avenues within CMC production to enhance broader areas of use such as characterization methods, and applications in aerospace, energy, and biomedical fields [22]. One current research project by Anthony *et al.* focuses on enhancing CMCs through novel reinforcements like graphene and carbon nanotubes (CNTs). Graphene-reinforced CMCs show promise in improving mechanical and electrical properties, but future research is still needed to optimize interfacial interactions and explore multifunctional applications [23]. Other future trends in CMC research include developing innovative processing methods, exploring new reinforcement materials, and optimizing crack-particle interactions for improved toughening mechanisms [24]. These advancements aim to expand the potential applications of CMCs and overcome current limitations in their performance and manufacturing.

Within AM, in addition to the overall research in the outcome product itself, research is targeted to components within the process. The aims of those efforts include, optimizing ink rheology, ink formulas, and printing parameters to improve the mechanical properties and structural integrity of printed CMCs. Other targeted research is focused on enhancing densities, improving mechanical properties, and developing structure-property correlations for AM-fabricated

ceramics [25].

Since the effectiveness of CMCs depends on their composition and manufacturing techniques, some research is being done showing promise in combining the two methods. One area of such work aims to overcome the geometrical inaccuracy seen in some AM parts. The traditional machining methods for CMCs, including grinding, ultrasonics, abrasive water jet, electrical discharge, and laser techniques, are being explored to balance material removal rates with minimizing surface damage [26]. Another combined area of work includes that with Lightweight CMCs (LCMCs). This type of CMC output is gaining attention for their high-temperature stability, low density, and corrosion resistance [27]. An article by O'Masta *et al.* combined digital light projection printing with pyrolysis to create silicon oxy-carbide CMCs [28].

Together, additive manufacturing and traditional manufacturing can be combined to achieve several different effects like densification of a part produced through AM via traditional techniques. Processes such as hot isostatic pressing (HIP), sintering, or chemical vapor infiltration (CVI) can be used to densify the part and improve its mechanical properties. Another option is to have AM create a tool or mold that can be used in traditional manufacturing methods. The processes can also be combined to create inserts or complex features on a pre-existing part produced via traditional methods or combining these methods to have AM repair and remanufacture a part produced through traditional methods. Lastly, the most popular combination seems to be for AM to produce a part and then use a traditional method, such as sintering or pyrolysis, to finalize the part. One such method combines the additive manufacturing technique of Direct Ink Writing (DIW) with the traditional manufacturing method of pyrolysis.

1.2 Direct Ink Writing

Direct Ink Writing (DIW) is an additive manufacturing technique that involves extruding a highly viscous ink or paste through a nozzle to create three-dimensional structures layer by layer. This method involves extruding viscoelastic inks through a nozzle allowing for the creation of filaments with various cross-sectional geometries [29]. The ink typically consists of a suspension of ceramic or polymer particles in a binder solution allowing it to retain its shape upon deposition. DIW enables the fabrication of complex geometries and customized parts with fine details and high precision. The process requires careful control of the ink's rheological properties to ensure consistent flow and solidification. Post-processing steps such as drying, de-binding, pyrolysis, and sintering, are often necessary to achieve the desired mechanical and structural properties in the final part. It is beneficial due to its low-cost, fast printing speed, and unique capability of aligning fibers in CMCs for enhanced mechanical properties [30].

1.3 Rheology for Ink Development

Rheology is the study of the flow of matter of various fluids and soft solids. It involves understanding how the material responds to applied forces, with a prevalent focus on properties such as viscosity, elasticity, and plasticity [31]. Rheological properties are essential in characterizing how materials behave under different conditions of stress, strain, and temperature. Rheology is important for DIW because it allows us to monitor changes in the ink formula viscosity properties, allowing us to optimize the ink formulation that is an ideal fit for DIW. Through optimizing the ink formula, we could find the appropriate ink that has (a) smooth extrusion through the nozzle by shear thinning behavior and (b) the crossover point so that the ink has dominant solid behavior and solidify quickly after deposition.

Rheology is tested by using an instrument commonly referred to as a rheometer. A rheometer is a tool that provides detailed information about a material's viscosity, elasticity, and viscoelastic behavior under various conditions of stress, strain, and temperature. There are multiple different types of rheometers, and they all have the capability of measuring the material's rheology just in different ways. One common rheometer is the rotational rheometer which uses either a cone-and-plate connection or a plate-and-plate connection. The cone-and-plate measures the torque required to rotate a cone over a flat plate with a thin sample layer between them. This test is typically done on small volume samples that contain a low viscosity (samples that flow more like liquid than a solid). The plate-and-plate connection does the same thing as the cone-and-plate, with the only difference being this connection uses two parallel plates to measure the material's response to shear. This connection is versatile and can accommodate different sample types and thicknesses. This is why the plate-and-plate connection will be used for all of the rheology tests throughout this project because the viscosity of an ink for DIW is difficult to control and can often bounce between high and low viscosity depending on which and how much additive is added.

The rheology of the ink for DIW must satisfy two criteria for a successful extrusion: (a) shear thinning and (b) structural stability through identifying the crossover point [32, 33]. These traits are tested by three corresponding tests which are as follows. (a) steady rate sweep (flow behavior) test which tests for shear thinning. Shear thinning means that when a shear stress is applied, the viscosity of the ink decreases so that it can flow under moderate pressures. The shear rate for the test can be conducted anywhere from 0.01 to 1000 1/s. Inks that possess these features are described by the Herschel-Bulkley model. (b) Oscillation amplitude sweep test

whose purpose is to see if the slurry has a dominant solid behavior after extrusion. The test is typically conducted at an oscillation strain range between 0.1% and 100%.

1.3.1 Steady Rate Sweep Test

The steady rate sweep test is a rheological test used to characterize the flow behavior of ceramic slurries used in the AM technique of Direct Ink Writing (DIW). For this test, the shear rate increases and decreases while analyzing the shear stress and viscosity of the slurry. This provides critical information about how the material behaves under different flow conditions and its shear-thinning or shear thickening behavior. For ceramic slurries, understanding the steady-state flow properties is crucial as the material must exhibit both flowability during extrusion and structural integrity after leaving the nozzle. Typical slurries for DIW exhibit non-Newtonian flow behavior, in that mainly the viscosity decreases (shear-thinning behavior) as the shear rate increases, allowing for smoother extrusion during printing. The steady rate sweep test gives the shear stress and viscosity results as important outcome measures of this behavior. However, these two parameters once graphed are not enough to determine the viscousity behavior of the slurry. To determine whether the slurry is shear thinning or shear thickening the graph must be modeled with the Herschel-Bulkley model, Figure 1 [34]. The Herschel-Bulkley model is a significant model to study and implement in relation to the creation of ceramic slurries. The Herschel-Bulkley model is a mathematical model used to describe the flow behavior of non-Newtonian fluids and especially of those that exhibit yield stress. This model incorporates a yield stress term which is an improvement of the classical Newtonian fluid model. The yield stress component is crucial in the formula as it identifies at what stress the fluid starts flowing. The Herschel-Bulkley equation is expressed in Equation 1 below, where τ is the shear stress, τ_θ is the yield stress, k is

the consistency index, $\dot{\gamma}$ is the shear rate, and *n* is the flow index. If *n*=1, the fluid behaves like a Bingham plastic, if *n* is greater than (>) 1 this indicates shear-thickening behavior, If *n* is less than (<) 1 this corresponds to shear-thinning behavior. This model is widely used in industries like food processing, cosmetics, and drilling fluids where the materials do not flow until a certain stress threshold is applied.

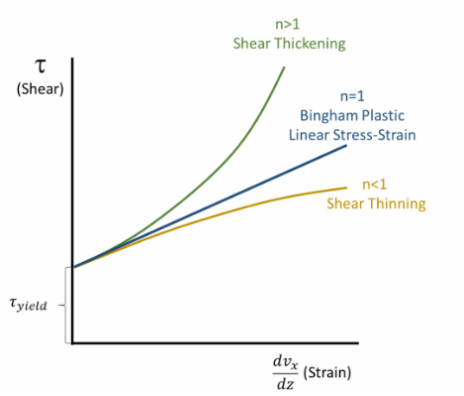

Figure 1 Herschel- Buckley Equation Graphed [34]

$$\tau = \tau_\theta + k\dot{\gamma}^{\,n} \qquad \text{Eqn. (1) [34]}$$

1.3.2 Oscillation Amplitude Sweep Test

The oscillation amplitude sweep test is a crucial rheological method used to determine the crossover point of materials such as ceramic slurries. In this test, the material is subjected to oscillatory shear deformation and the amplitude of strain is incrementally increased while keeping the frequency constant. The goal is to evaluate how the storage modulus (G′) and loss modulus (G″), which represent the elastic and viscous properties of the material respectively. The crossover point helps to identify the point where the ink/slurry goes from exhibiting solid-like behavior to liquid-like behavior. This point is used to help determine the printability of the

ceramic slurry.

As depicted in Figure 2, the amplitude sweeps test reveals three distinct regions, which help define the material's transition from solid-like to liquid-like behavior [35]. In the white region, corresponding to the linear viscoelastic region (LVR), G′ is higher than G″ signifying that the material is primarily elastic with a solid-like response to deformation. This region is crucial for determining the yield point (Point 1 in Figure 2), where the material first begins to yield but still retains its structure. Here, G′ remains constant, and the material behaves in an elastic manner, meaning it can recover after deformation.

In the grey region, of Figure 2, the graph shows that G′ begins to decrease as the strain amplitude increases, indicating internal structural breakdown. This is the point where the elastic modulus G′ and the viscous modulus G″ intersect (Point 2), marking the transition from a solid-like to a more liquid-like behavior. This point is often referred to as the flow stress point, where the material starts to exhibit more viscous properties and loses its internal structure, shifting toward flow-like behavior. Finally, in the blue region, G″ surpasses G′, indicating that the material is now predominantly in a liquid-like state. This flow region shows the material's behavior at high strain, where it flows more easily, and its internal structure is fully broken down.

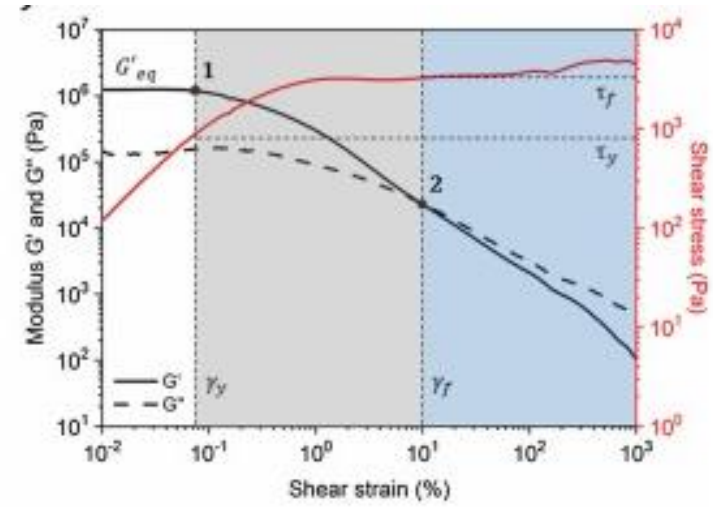

Figure 2 Amplitude Sweep Test [35]

The oscillation amplitude sweep test is essential for understanding the viscoelastic properties of materials, particularly in manufacturing processes like Direct Ink Writing (DIW), where materials need to transition from a stable, solid-like state to a flowable, liquid-like state without losing structural integrity too early. These three regions help define the material's mechanical stability and flow characteristics under different strain conditions.

1.4 Pyrolysis

Pyrolysis is a thermal decomposition process that involves heating a material in the absence of oxygen causing it to chemically decompose into smaller molecules. It is commonly used to convert organic materials, such as polymers, into gases, liquids, and solid residues often leaving a carbon-rich solid. In the context of ceramic matrix composites (CMCs), pyrolysis is used to transform polymer precursors into ceramic phases forming a ceramic matrix. The process typically occurs at high temperatures, ranging from 900°C to 1500°C, depending on the material and desired properties [36, 37]. Pyrolysis is crucial in manufacturing advanced materials, such as

converting polymer infiltrated preforms into fully ceramic components.

Hence in this study the goal will be to develop a protocol for SiC/C CMC ink design and preparation by considering appropriate rheological properties and printability for DIW process, pyrolysis, and characterization.

1.5 Recent studies on DIW of CMCs

While direct ink writing has been shown to be low cost and fast, and has greater mechanical properties [38, 39]DIW is still in its infancy especially when it comes to the printing and creation of CMC inks. The difficulty is that these CMC inks tend to be highly viscous [39] and due to the number of additives that could be present within the ink it becomes difficult to balance the viscosity with an optimal result.

Successful ink formulations that have been used in previous studies include an Aluminum Oxide (Al_2O_3) matrix with Silicon Carbide (SiC) fiber reinforcement [40], a Zirconium Diboride and Silicon Carbide (ZrB_2-SiC) matrix with carbon fiber (C_f) reinforcement [41], and for the majority of studies a SiC matrix with C_f reinforcement appears to be one of the main combinations used regardless of the printing and traditional methods used post print [42-45]. This is why CMCs consisting of a SiC matrix and C_f (SiC/ C_f) reinforcement was selected as a model system recipe from literature [39].

A preceramic polymer is an important additive to use within DIW ink formulations as a preceramic polymer determines what ceramic matrix will be produced upon pyrolysis. The preceramic polymer poly(methyl-silsesquioxane) (PSMQ), also referred to as Silres MK powder is a common type of preceramic polymer used to create the SiC matrix within ceramics [46]. The

solvent component in ink formulations primarily used is isopropanol alcohol (IPA). The solvent serves multiple roles within ink formulation from controlling viscosity to being integral to the inks drying behavior [47]. The inert filler in the formulas is SiC powder Starceram S Grade UF 10 and serves two purposes. The first purpose is to allow the ink to turn more solid and the second is to give the preceramic polymer something to latch onto during the pyrolysis process allowing the SiC matrix to form more easily [39]. In addition to the above formula ingredients, things such as a reinforcement agent liked chopped carbon fibers can be added to the ink formulation for the purpose of enhancing the final mechanical properties of the CMC. As rheology is a crucial aspect of ink formulation certain additives such as hydrophobic fumed silica Aerosil R106 are used as rheology modifiers. With the fibers, fillers, and other modifies, a dispersing agent like BYK 180, can be used to allow for the particles within the ink formulation to be evenly distributed in the ink. The addition of a crosslinking agent, such as Geniosil GF91, will allow the shear-thinning behavior and rapid viscosity recovery of the ink for a successful DIW. Crosslinkers also can help align the reinforcement along the printing direction due to shear stresses at the nozzle tip. This will potentially improve the mechanical properties of the final composite [20, 39]. These crosslinking agents will also help during pyrolysis allowing for the matrix to be formed easier during traditional manufacturing methods.

The pre- and post-processing of CMCs are distinct from polymers. CMCs can be fabricated using polymer pyrolysis, where organometallic polymers serve as precursors to ceramic matrices, offering low-temperature processing without fiber degradation [48, 49]. Pre-processing of CMCs involves raw material preparation, forming techniques, and infiltration, followed by thermal treatment of preceramic polymers, which modifies properties such as molecular weight

distribution, viscoelastic state, and ceramic yield [50]. The polymer precursor approach allows for tailoring of reinforcements, matrix precursors, and fillers [49]. Post-processing may include de-binding, pyrolysis, sintering, infiltration and densification, and the application of barrier layers between fibers and matrix to improve composite performance and prevent catastrophic failure [51]. In contrast to polymer composites, CMCs exhibit brittle behavior which can be altered through careful processing techniques. Understanding these processing differences is crucial for optimizing CMC properties and expanding their potential applications.

Considering that the rheology of the inks is the key factor for the DIW process and is crucial for the fabrication of geometries able to retain their shapes; this work will start with the basis of two successful preceramic polymer ink formulations and test for outcomes with the three most important additives within the ink's design. The work will also include trying to determine the unclear ratio of fiber dimension and weight ratio and initial pyrolysis testing outcomes of the product that may simulate real world outcome applications. The rest of this thesis paper will contain: the methods section discussing the ink formulations and modifications, the rheology testing parameters and the pyrolysis testing parameters. This will be followed by the results and discussion section that presents the results of testing, adaptations and retesting and implications from the testing results.

CHAPTER 2: MATERIALS AND METHODS

2.1 Materials

Many materials that will be used to make the ink formulations for this study originate from a paper by Franchin et. al. [20, 39]. This work was chosen for its formulas designed to contain two crucial properties for DIW. The first property is that the ink had a very fast crosslinking time which can improve the behavior of the final ceramic product. The second property that this ink exhibited was that it allowed for a lower processing temperature. This lower processing temperature is significant as it will decrease the time that it will take for a completed part to be created. What a lower processing temperature means is that rather than fully melting the part through sintering, a less heat intensive process called pyrolysis is used to turn the sample into a ceramic.

The ink formula uses numerous additives as listed in the previous section. Our study uses similar materials to the study conducted by Franchin et. al., represented in Figure 3 and include, Silres MK powder (bought from Wacker Chemie AG) a type of poly(methyl-silsesquioxane)) used as the preceramic precursor. In addition, isopropanol alcohol (IPA) is the solvent, SiC powder Starceram S Grade UF 10 (bought from abcr GmbH) is the inert filler; BYK 180 (bought from BYK Additives & Instruments) is the dispersing agent. Some milled, uncoated AGM99MF0150 PAN fiber (bought from Asbury Carbons with a length of 150 μm, a diameter of 7-9 μm, and a carbon content of 99%) was used as reinforcement. Hydrophobic fumed silica Aerosil R106 (bought from Evonik Industries) was used as the rheology modifier, and Geniosil GF91 (bought form Wacker Chemie AG) was included as the crosslinking catalyst.

Figure 3 Ink Formula Ingredients

2.2 Methods and Equipment

2.2.1 Slurry Creation

The equipment used in the creation of the slurry creation is depicted below in this section, Figure 4 (a-d). The equipment used is a 50 milliliter (mL) beaker, Figure 4(a), that is used to hold and mix all the additives together. Another piece of equipment that was used is the Slender Magnetic Stirrer Hot Plate Mixer, Figure 4(b), capable of reaching temperatures of 550 °C and speeds of up to 2000 rotations per minute (RPM). This mixer was used to initially stir all the additives together within the beaker. The stirrer worked by placing the beaker on top of a metal platform, and dropping in a pill shaped plastic device that had a magnet located in its center. Once the magnet is at the bottom of the beaker the machine can be turned on and it will start spinning the pill shaped device creating a strong spinning effect. However as described in later sections this magnetic stirrer was replaced with a high shearing mixer, the Cole-Parmer OS-200D-C-SYS Compact Digital Mixer System, Figure 4(c), to better mix this slurry given its thickness. This device works by spinning a rod with fins attached to the end, to break up any agglomerates that might form since it can reach speeds up to 2500 RPM. The last piece of equipment used in the creation of the slurry was the Ohaus Pioneer Model PX124 Analytical Balance Scale, Figure

4(d). This scientific scale has a 120-gram (g) weight capacity, is readable to 0.0001 g, and contains internal calibration equipment.

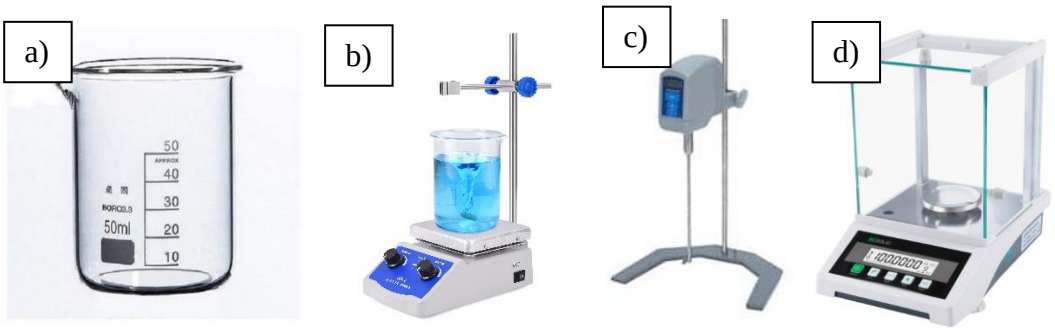

Figure 4a-d Slurry Mix Equipment a) 50 milliliter (mL) beaker, b) Slender Magnetic Stirrer Hot Plate Mixer, c) Compact Digital Mixer System, and d) Ohaus Pioneer Model PX124 Analytical Balance Scale.

2.2.2 Rheology

The main pieces of equipment used to measure the rheological properties of the inks is the TA Instruments Q800 Dynamic Mechanical Analyzer and the TA Instruments AR2000ex Rotational Rheometer, Figure 5 and Figure 6 respectively.

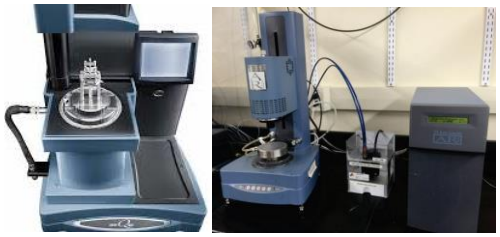

Figure 5 (left) and Figure 6 (right) Rheology Equipment

The TA Instruments Q800 Dynamic Mechanical Analyzer (DMA) is an advanced instrument

used to measure the mechanical properties of materials under dynamic loading conditions. Its purpose is to analyze the viscoelastic behavior of various materials over a range of temperatures and frequencies. The DMA is known for its high sensitivity, precision, and versatility. It can measure properties such as storage modulus, loss modulus, tan delta, and creep compliance. The DMA uses a variety of attachments to measure the above properties, including dual and single cantilever clamps, tension clamps, and shear sandwich clamps. Each of these attachments is used for different testing modes and materials. The DMA can also conduct mechanical tests, such as the three-point bending, tension, and compression tests.

The TA Instruments AR2000ex Rotational Rheometer is designed to characterize the flow and deformation behavior of complex fluids and soft solids. This rheometer can measure a wide range of rheological properties including viscosity, yield stress, thixotropy, and viscoelastic moduli. It operates over a wide range of shear rates and stresses. These traits means it used in a number of applications for industries such as food, pharmaceuticals, cosmetics, polymers, and research. The AR2000ex can perform both controlled stress and rate experiments providing comprehensive insights into the material's rheological behavior. The AR2000ex is equipped with various geometries including cone-and-plate, parallel plate, and concentric cylinder, enabling it to handle a wide range of sample types and viscosities. Additionally, it can be outfitted with environmental control systems such as Peltier plates and fluid baths to maintain precise temperature conditions during testing. This allows for the study of temperature-dependent rheological properties and the assessment of material behavior under realistic application conditions.

Together, these instruments provide a thorough characterization of material properties, enabling

researchers and engineers to understand the mechanical and rheological behavior of materials under various conditions. This understanding is crucial for material selection, quality control, and the development of new materials with tailored properties for specific applications.

All three tests section (steady rate sweep, oscillation amplitude sweep, and oscillation frequency sweep test) used the parallel plates attachment and were cleaned before moving on to the next test. The steady rate sweep test was the first test conducted with the following parameters, Shear rate - 0.1 to 1000 1/sec. The second, oscillation amplitude sweep, test was conducted with the parameters: Oscillation strain - 1 to 100% and was conducted at a frequency of 1 Hertz (Hz). The last test that was conducted was the oscillation frequency sweep test and was conducted with a 1% strain at angular frequencies ranging from 0.1 to 100 rad/sec. These parameters are consistent with those from the literature [20, 39]. All these tests were conducted at 20 ℃ (room temperature) using a 20 mm parallel plate geometry attachment.

2.2.3 Printing

The printing of samples used in this paper will be done through two different methods. The first method is used to produce large multi-layered samples using the commercial Tronxy Moore 2 Pro DIW printer, Figure 7. The second method uses a do-it-yourself (DIY) syringe extruder, Figure 8, used to make single layer samples. The setup was assembled by the author and the plastic piece was 3D printed, following the open-source guideline [52].

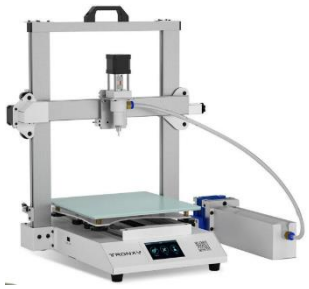

Figure 7 DIW Printer

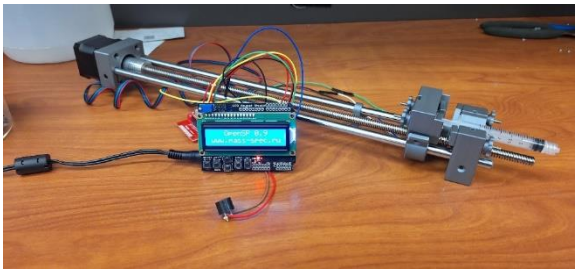

Figure 8 Assembled Syringe Extruder

The Tronxy Moore 2 Pro is a ceramic and clay DIW printer produced by Tronxy 3D Printers. This printer differs from traditional 3D printers that use plastic filaments as it is engineered to handle the unique properties of viscous paste-like materials such as ceramics, clay, and other composite slurries. One important feature of the Moore 2 Pro is its large build volume of 255 millimeter (mm) long by 255mm wide and 260 mm high allowing for the creation of sizable objects in a single print.

The Tronxy printer is designed with three primary subsystems, the barrel, the extruder, and the stage. The extruder subsystem consists of two key components. The reservoir, which stores the ceramic slurry and the extrusion mechanism, which applies pressure to drive the slurry through the nozzle system. The nozzle system is mounted to the stage and precisely controls the deposition of the ceramic slurry onto the build plate. The stage serves as the central platform of the printer, is where the build plate is positioned, and where the entire printing process takes place. This design allows the fabricated part to be constructed layer by layer with high precision.

The printer is equipped with an advanced extruder system, as shown in Figure 9, specifically engineered to handle the high viscosity of ceramic and clay materials, ensuring a smooth and consistent extrusion process. This extruder system is designed to maintain precise control over

the material flow, which is essential for producing high-quality prints with intricate details. The ceramic slurry is initially loaded into a clear plastic tube, which is then securely attached to the silver component housing the plunger mechanism within the vice. A small gold and blue connector is subsequently screwed onto the tube's end allowing a flexible tube to be attached. This flexible tube is connected to a corresponding gold and blue connector facilitating the transfer of the ceramic slurry from the barrel to the nozzle. The black component in the center of the silver piece is the plunger which is connected to a long lead screw. Upon entering the printing parameters, the lead screw rotates driving the plunger forward. This action gradually pushes the ceramic slurry out of the barrel through the flexible tube and into the nozzle where it is precisely deposited onto the build platform. This controlled extrusion process is vital for maintaining the integrity and accuracy of the printed object.

Figure 9 Printer Extrusion System

The nozzle system, as depicted in Figures 10 and 11, is designed to accommodate various nozzle sizes. This allows users to optimize both the resolution and print speed based on the specific requirements of their project. Upon entering the system through the white cylindrical component

shown in Figure 8, the ceramic slurry is directed into a precision lead screw mechanism integrated with the motor. This lead screw applies controlled mechanical force, driving the slurry downward through the system. The slurry is then subjected to shear forces within the extruder, which facilitates its extrusion through the nozzle (illustrated as the rightmost silver component in Figure 8) onto the build plate. This process ensures accurate deposition of the material, essential for achieving the desired structural and surface characteristics of the printed part.

Figure 10 (left) and Figure 11 (right) Printer Nozzle System

The stage of the Tronxy Moore 2 Pro, as illustrated in Figure 12, is engineered with a robust frame and an integrated heated build platform which is critical for maintaining precise temperature control during the printing process. This temperature regulation is essential for preventing material deformation which can include things such as warping or cracking common in temperature-sensitive materials like ceramics. The stage also serves as the mounting point for the nozzle system, facilitating its precise movement across the build area. This system enables the controlled deposition of the ceramic slurry layer by layer, ensuring the accurate fabrication of complex 3D components.

In terms of software, the Moore 2 Pro is compatible with a variety of slicing programs that allow users to prepare their 3D models for printing. The software includes settings tailored for ceramic

and clay printing helping users optimize their prints for these specific materials. The main software program used in this study is Ultimaker Cura slicing software. Additionally, the printer supports connectivity options such as USB and SD card inputs, making it easy to load and manage print files. Overall, the Tronxy Moore 2 Pro Ceramic & Clay 3D Printer is a powerful tool for anyone looking to explore the creative possibilities of 3D printing with non-traditional materials. Its specialized design, combined with user-friendly features, makes it an excellent choice for producing high-quality ceramic and clay objects, whether for artistic, industrial, or functional applications.

There were some limitations. The components of the Tronxy Moore 2 Pro are small, particularly those involving the nozzle subsystem. This leads to them being very difficult to clean out once the ceramic and clay start to dry. This is why two cleaning tools were needed to help clean out the components once printing was finished. This first was the VEVOR Professional Ultrasonic Cleaner, Figure 12, which is used to break up and soften the hardened material in the smaller pieces. An ultrasonic cleaner operates by using high-frequency sound waves to clean objects submerged in a liquid. This device generates ultrasonic waves, around 40 kHz, which are transmitted through the liquid. These sound waves create microscopic bubbles in a process known as cavitation. When the bubbles collapse or implode, they produce tiny shock waves that dislodge contaminants from the surfaces of the submerged objects. This process effectively removes dirt, grease, and other impurities from intricate parts, including those with complex geometries or delicate surfaces, without causing damage. Ultrasonic cleaning is widely used in various industries, such as jewelry, electronics, and medical equipment, due to its efficiency, precision, and ability to clean without the need for harsh chemicals or mechanical scrubbing.

Figure 12 Ultrasonic Cleaner Figure 13 Water Flosser

The second equipment used to clean the printer was the Waterpik Cordless Water Flosser, Figure 13. This cordless water flosser is used in this study to clean out the nozzle as depicted in Figure 10. The nozzles used can be less than 0.1 mm in diameter, so by using the ultrasonic cleaner to soften the clay, the water flosser is then used to force the softened clay out of the nozzle. The water flosser works by pressurizing water in a reservoir and directing it through a small nozzle, creating a pulsating jet of water. This stream effectively dislodges any ceramic from the inside of the nozzle.

The DIY syringe extruder was the second type of extrusion device used. During the study it was found that making a single layer sample was difficult with the Tronxy DIW printer for fast pyrolysis analysis. Smaller samples were necessary as they could be used as indicators to how the large samples would perform under the same pyrolysis conditions. The nozzles of the Tronxy DIW printer were found to fit on the end of a 3 mL syringe. This allowed single layered samples to be created easily and with less materials. The syringe extruder is designed for use in an analytical laboratory and offers several advanced features. This extruder includes a universal clamp that accommodates various syringes with diameters up to 25 mm. It also allows users to adjust all key parameters such as syringe diameter, flow rate, target volume, and time directly via a control panel with buttons and a two-line display. This eliminated the need for a computer

connection. The pump supports infusion, refilling, and continuous cycle modes with dispensing accuracy and reproducibility on par with commercial syringe pumps. Users can change units for volume, flow rate, and time, and any illegal input values are automatically rounded to the nearest valid value. Additionally, all settings are saved in non-volatile memory and the pump can be assembled in just a few hours with minimal soldering required. The syringe extruder was made with a mount so that it can be easily mounted onto the stage.

During the extrusion process to save time and resources, only enough of each solution was prepared to make 8-10 samples from a 3 mL syringe. Originally the samples created with the syringe were uneven and it was hard to maintain a consistent height all the way through as the samples were being deposited by hand. This issue was solved with the replacement of a DIY syringe extruder. This device allowed the inks to be extruded at a constant pressure rather than the variable pressure presented when doing it by hand. The issue of maintaining constant height and speed was solved through the creation of a custom mounting device shown in Figure 14. This custom mount allowed the DIY syringe extruder to travel at a constant speed. And as the printer's z-axis limit switch has an adjustable height it allowed for a constant height if the printer ran in a straight line.

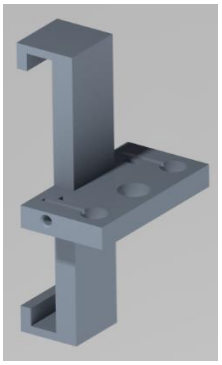

Figure 14 Custom Mounted device for Syringe Extractor

In this study, a typical set of printing parameters is that the nozzle used to print the samples has an inner diameter of 1.9 mm; the ceramic slurry was extruded out of the nozzle at a speed of 0.033 mL/sec, and printed at a height of ~2mm and at a print speed of 15mm/s. The sample lengths varied but were generally between 10mm and 50mm in length. The samples dried for 24 hours before being put into the furnace.

2.2.4 Heat treatment

The one piece of equipment that will be used to pyrolyze the samples is the SentroTech: ST-1800C-445 High Temperature Box Furnace, Figure 15. The SentroTech furnace is a precision-engineered device designed for advanced material processing and testing capable of reaching a maximum continuous operating temperature of 1800 °C. This high-temperature capability is crucial for applications requiring extreme heat such as sintering, annealing, or conducting materials research. The furnace features a compact heating chamber measuring 4 inches wide, 4 inches high, and 5 inches deep, which is ideal for small-scale experiments or processing high-value materials in controlled environments. The furnace is equipped with a Eurotherm Nanodac controller allowing for sophisticated thermal management with the ability to program up to 100 different heating profiles, each with 20 segments. This advanced control system ensures precise temperature regulation and repeatability making it suitable for complex thermal processes that require meticulous temperature control. The heating element, sized at 6/12, is designed to efficiently deliver power while maintaining uniform heat distribution within the chamber. Operating at 3 kW of power and requiring a single-phase voltage of 208/240 V, the furnace is both powerful and energy-efficient, making it suitable for laboratory or small-scale industrial settings. The use of a Pt20Rh/Pt40Rh (Platinum-Rhodium) thermocouple enhances the furnace's

temperature measurement accuracy and reliability, which is essential for maintaining the desired thermal conditions. Additional features include an exhaust port for safe removal of gases generated during heating and a nitrogen/argon purge kit which allows for an inert atmosphere within the chamber. This capability is critical for processes that require the exclusion of oxygen to prevent oxidation or contamination, further broadening the furnace's range of applications in materials science and engineering.

Figure 15 Pyrolysis Furnace

2.2.5 Characterization

There are two machines that will primarily be used for the characterization of samples produced. The first machine used is the thermo-gravitational analysis (TGA) machine. The TGA testing machine is a highly specialized instrument used to measure the changes in the mass of a material as a function of temperature or time under controlled atmospheric conditions. The core principle of TGA involves placing a small sample of the material on a precision balance within a furnace chamber. As the furnace gradually heats the sample, the machine continuously monitors and records the sample’s weight. The changes in mass can indicate various thermal processes, such

as decomposition, oxidation, or volatilization. The TGA system is equipped with a highly sensitive microbalance capable of detecting minuet changes in mass, often in the microgram range, ensuring precise measurements. The furnace is programmable, allowing for controlled heating rates and temperatures, which are crucial for studying specific thermal behaviors. Additionally, the machine often includes the ability to introduce different gases into the chamber such as nitrogen, oxygen, or inert gases, to simulate various environmental conditions or to prevent oxidation during the analysis. The data collected from a TGA test can be used to determine a material's thermal stability, composition, and reaction kinetics, making it a valuable tool in materials research, quality control, and development of new materials.

Thermo-gravimetric analysis (TGA) plays a critical role in characterizing ceramic slurry by providing detailed insights into its thermal stability, composition, and behavior under different temperature conditions. When applied to ceramic slurry, TGA measures the mass loss of the slurry as it is gradually heated. This reveals the presence and quantity of volatile components, such as water, organic binders, and dispersants. As the temperature increases, these components evaporate or decompose, leading to observable weight changes. By analyzing these weight loss patterns, TGA can determine the precise temperatures at which these processes occur, offering valuable information about the drying and firing stages of the ceramic material. Additionally, TGA helps identify the decomposition of any organic additives used in the slurry formulation, which is essential for optimizing the ceramic processing parameters to achieve desired properties in the final product. This characterization is crucial for ensuring the quality and consistency of ceramic materials, particularly in industries where precise thermal behavior is necessary for achieving specific mechanical and structural properties. Ink A was the only formula that was

used for TGA testing as it contained all the additives used in the study. The TGA test was performed in the conditions described in Table 1. For this test, the sample was broken down into a sample ~2-3 mm in length, placed into a small ceramic crucible, and then carefully lowered into the main body of the TGA testing machine.

Table 1 TGA Testing Parameters

Ink	Max Temperature (℃)	Ramp Rate (℃/min)	Environment
A	1100	10	Air

The second machine used in this study is the Scanning Electron Microscope (SEM) JEOL model JSM-6480 machine, Figure 16. Due to its ease of operation and maintenance, SEM is one of the most widely utilized tools for analyzing nanostructured materials. SEM images are generated by scanning the surface of a specimen, providing detailed information about the specimen's topography and chemical composition. The primary components of an SEM include an electron gun, electromagnetic lenses and apertures, scanning coils, detectors, and a vacuum system, as illustrated in the schematic diagram below. Figure 17 depicts the electron gun positioned at the top of the column which generates a beam of electrons by applying an acceleration voltage between the electron source (acting as a cathode) and the anode plate. The acceleration voltage in an SEM typically ranges from 1 to 40 kV.

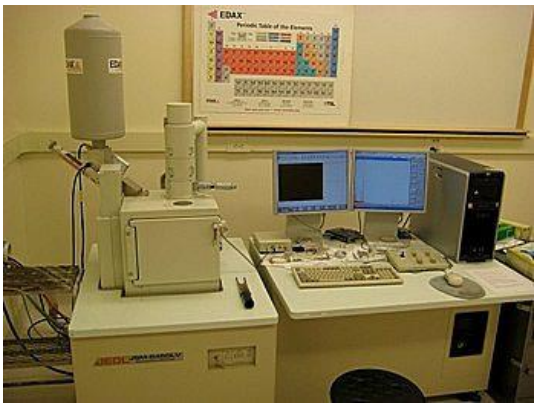

Figure 16 Electron Microscope

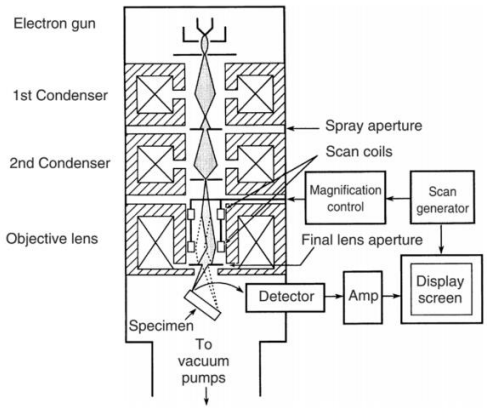

Figure 17 Electron Gun

When an electron beam interacts with a specimen in a scanning electron microscope (SEM), it generates signals such as secondary electrons (SEs) and backscattered electrons (BSEs), each revealing different aspects of the specimen's surface and composition. SEs, produced from near-surface interactions, provide detailed surface topography while BSEs, generated by elastic scattering, offer compositional contrast with materials of higher atomic numbers appearing brighter. To capture these signals, SEMs use detectors like the Everhart-Thornley (E-T) for SEs and specialized detectors for BSEs. High-resolution imaging in SEMs requires optimizing parameters such as acceleration voltage, working distance, and spot size. In this study, a working distance of 10 mm, and an acceleration voltage of 5-30 kV were used in order to achieve better results.

This sample was then put onto the strip of double-sided copper film that was adhered to the SEM sample platform. To get a good measure of the other characterization properties, an image of the cross section was needed. To get that, the sample is held up and a small section is broken off and discarded. Breaking off this discarded section is important as the sample needs to be upright to preserve the fibers and so that no loose or broken fibers will fall on out. The upright sample is

now carefully broken again with a pair of tweezers into a segment less than or equal to 5 mm and placed onto the double-sided copper tape. This process was repeated to get both the surface and cross-sectional images for all the samples. The sample platform was then loaded to the SEM machine and images were taken using the JEOL software.

CHAPTER 3: RESULTS AND DISCUSSION

3.1 Slurry Creation

Inks C through F had varying amounts of SiC powder with MK solution mixed in. Results showed that Ink C had the highest concentration of SiC, but turned out to be unsuitable for DIW because the mixture was too viscous. Inks D, E, and F, containing progressively lower concentrations of SiC exhibited increased liquid like behavior as the amounts of the SiC decreased. This reduction in viscosity allowed for easier mixing and therefore testing potential was possible. The balance between SiC powder and the MK solution therefore does seem to exhibit a crucial role in determining the viability of an ink formulation for smooth extrusion and deposition in additive manufacturing processes.

Since Inks D and F contained the lowest and highest *n* value for shear thinking behavior respectively, they were modified with fumed silica to create inks G and H. Fumed silica was added at the cost of the amount of SiC powder to Inks D and F to test the two extremes of the rheology properties observed in the previous tests (shear thinning and shear thickening behavior). The addition of fumed silica did not appear to have a significant effect on Ink D. However, when added to Ink F, fumed silica created an increased viscosity requiring more mechanical power to stir the solution. This was believed to be a sign that the rheology and suitability of Ink F was improved by the addition of fumed silica.

The last set of ink formulas to be mixed were those containing the first type of fibers bought from Asbury Carbons. Inks I thought K were modified from Ink E based on rheology results and included the fumed silica from Inks G and H. The carbon fibers were added in 5 wt. % intervals to the ink formulas at the cost of SiC powder. The addition of these carbon fibers did not have a

noticeable/measurable impact at the mixing stage of the ink development.

The creation of the ceramic slurries was motivated from the study of Franchin *et. al.* [39]. As shown in Table 2, IPA is the solvent, MK and SiC are the core ingredients, fumed silica is the rheology modifier and dispersant BYK180 is the crosslinking agent. In our study, since cross-linking (curing time) takes about two hours and creates a challenge for DIW writing processes as it can take longer, cross-linking agent was removed.

Table 2 Ink A and B formulas with amounts of additives plus dispersant

Ink	IPA (mL)	MK (g)	SiC (g)	Carbon Fibers (g)	Fumed Silica (g)	Dispersant BYK180 (mL)
A	9	21	17.85	5.35	2.68	1.15
B	9	21	14.88	5.95	N/A	0.75

To explore the role of individual additives, we have design different set of experiments. Tables 2-5 are tables that are used to explore and highlight each individual additive's effects on the slurry throughout the ceramic creation process. Exploring each individual additive also helps to narrow down the optimal range of each additive that should be added to the slurry. Table 3 is used to focus on the role that SiC inert fill can play in the slurry. Table 4 focuses on the role of fumed silica while Table 5 focuses on the impact of the first type of carbon fibers. Each table includes a column labeled 'IPA+MK,' which specifies the amounts of isopropyl alcohol (IPA) and MK polymer precursor added to each slurry formula. This column provides a breakdown of how much MK+IPA solution is added to each ink formula. Additionally, each ink formula listed in the tables contains a dispersing agent to ensure even distribution of particles within the slurry.

This dispersing agent is added in by ~2.45% of the solid weight percentage in each formula.

Table 3 SiC slurry formulations

Ink	IPA+MK (wt. %)	SiC (wt. %)
C	35	65
D	45	55
E	55	45
F	65	35

Table 4 Fumed Silica slurry formulation

Ink	IPA+MK (wt. %)	SiC (wt. %)	Fumed Silica (wt. %)
G	45	50	5
H	65	30	5

Table 5 Carbon Fibers type on slurry formulation

Ink	IPA+MK (wt. %)	SiC (wt. %)	Fumed Silica (wt. %)	Carbon Fiber #1 (wt. %)
I	55	35	5	5
J	55	30	5	10
K	55	25	5	15

The first step is creating the IPA+MK solution to be the base of each formula. This process

mixture is created by mixing IPA and MK powder in a weight ratio of 30:70, respectively in the 50 mL beaker. The MK powder is mixed into the IPA using the high shearing mixer at speeds ranging from 800-1000 RPM. Once all the powder is successfully integrated into the IPA, the mixture is stored in an air-tight bottle to prevent hardening and left for 24 hours to allow for all the air bubbles to settle out of the mixture. This solution is what is added for the IPA+MK column seen in all the tables above and is used as the base of the ceramic slurry.

3.2 Rheological properties of inks

The objective for rheological property investigation is to understand the behavior of ink during and after DIW. Shear thinning behavior is the first focus for the slurry, which is tested by steady rate sweep. As point out by Franchin et al, this type of inks lack in adhesion to the rheometer plates, which tend to be expelled from the side even at low shear rates (above 10 1/s), which doesn't cover the shear rate during printing (50 - 100 1/s). Therefore, in addition to steady rate sweep, dynamic oscillation tests allowed us to assess whether the inks had a transition to low rigidity systems at higher shear stress values.

3.2.1 Rheological Behavior of Reference Inks (A and B) – Role of FS

The first test that was conducted was the steady rate sweep test 0.1 to 1000 1/sec shear rate. The results of the test were plotted and fitted to the Herschel-Bulkley model to determine the shearing behavior of the two inks, in Figure 18 and 19 below. Where Figure 18 represents Ink A and Figure 19 represents Ink B. The black line in both figures represent the data recorded from the rheology test and the red line is the Herschel-Bulkley fitted line. Analyzing the fitted line, it becomes possible to determine the individual values of the Herschel-Bulkley model, giving an *n*

value of 0.39 and 1.32 for Inks A and B respectively. Since Ink A returns an *n* value less than one it is suitable for DIW, however since Ink B's *n* value is greater than 1 this means Ink B is not suitable for DIW.

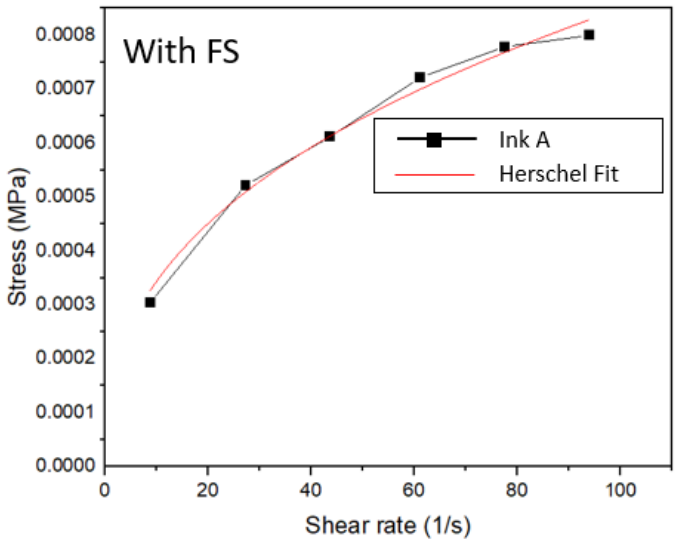

Figure 18 Steady Rate Sweep Test of Ink A

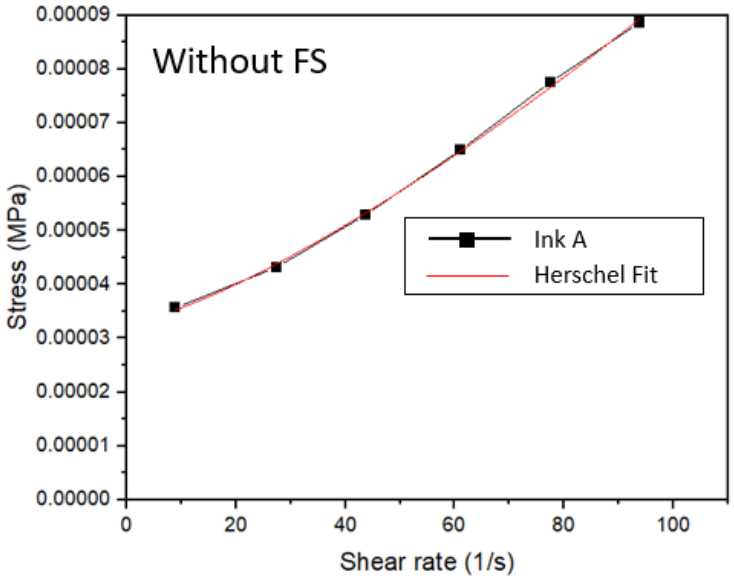

Figure 19 Steady Rate Sweep Test of Ink B

The next test conducted on Ink A and B was the oscillation amplitude sweep test to determine if a crossover point exists, Figure 20 and 21 respectively. For Ink A, Figure 20, the results show how the slurries viscoelastic properties change with increasing oscillation strain. At low strain levels (up to ~10% strain), the storage modulus (G') is higher than the loss modulus (G"), indicating that the ink behaves predominantly like a solid. This behavior is ideal for maintaining shape after deposition during DIW. As seen on Figure 21, as the strain increases into the range of 10–50% strain, G' begins to decline while the G" remains relatively constant, indicating the start of structural rearrangement within the slurry. This area represents the ink's yield point, where it starts transitioning from solid-like behavior to more fluid-like properties. Beyond the 50% strain point of the graph, both G' and G" decrease sharply. This indicates that the ink undergoes complete structural breakdown becoming predominantly viscous and capable of flowing easily at high strains. In conclusion, Ink A exhibits an ideal combination of solid-like behavior at low strains. This is crucial for shape retention in DIW applications and fluid-like behavior at higher strains as it allows for smooth extrusion. The yielding behavior observed around 10% strain is critical for determining the ink's printability ensuring it can flow when needed while maintaining structural integrity after deposition.

The oscillatory amplitude sweep test for Ink B, Figure 24, reveals at low strains (up to ~1%), the G' is slightly higher than the G", indicating that the ink behaves predominantly like a solid, with elastic properties dominating. As strain increases beyond 1%, the G' begins to decline significantly, while the G" decreases at a slower rate. This marks the beginning of structural breakdown, as the ink transitions from solid-like to more viscous behavior. In the higher strain range (beyond ~10%), the G' drops sharply by an order of magnitude, while the G" remains

higher, indicating that the ink is behaving predominantly as a viscous material. In conclusion, Ink B shows a transition from elastic to viscous behavior as strain increases. While it retains solid-like properties at low strains, it begins to yield and flow more easily beyond 1% strain. At higher strains, the ink experiences significant structural breakdown and becomes more liquid-like. Compared to Ink A, Ink B has a lower resistance to deformation, which suggests it may flow more easily during printing but may struggle to maintain its shape after deposition. The only noticeable difference between these two inks is that Ink A used fumed silica while Ink B did not. This leads to a possible outcome that the implementation of fumed silica can help improve and extend a slurries crossover point. Based on this conclusion, due to the smaller crossover point in Ink B, it is believed that Ink A makes for a more suitable slurry for DIW use.

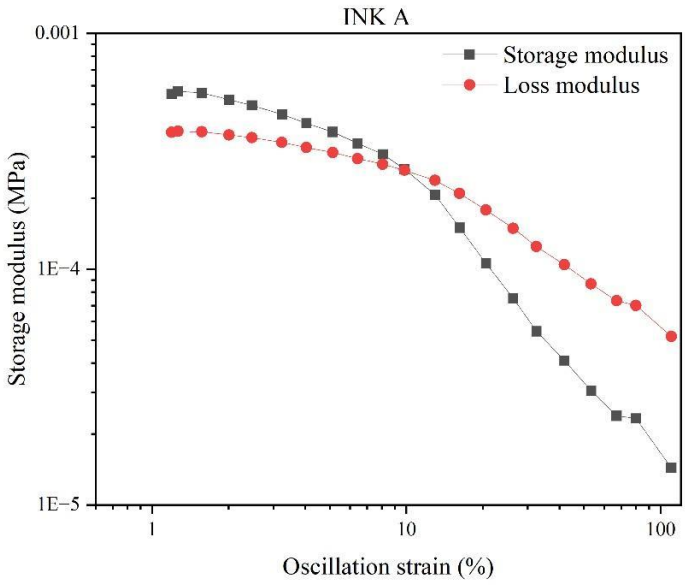

Figure 20 Oscillation Amplitude Sweep Test of Ink A

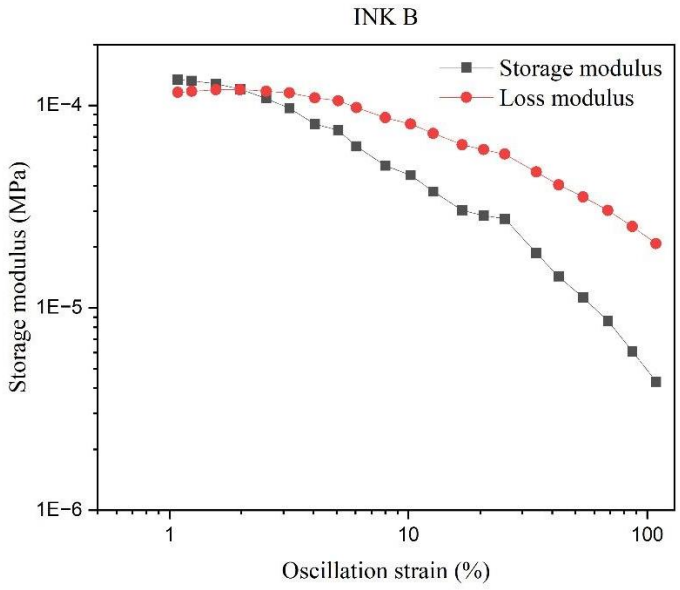

Figure 21 Oscillation Amplitude Sweep Test of Ink B

Based on the two rheology tests conducted it is believed that FS plays a crucial role in the steady rate sweep test, in that without FS the ink will not exhibit the shear thinning properties, which are crucial for DIW. FS also extends the crossover region from as seen in results from the amplitude sweep test, meaning that fumed silica can improve the structural stability of the Ink. In SiC-based ceramic slurries, FS particles contribute to shear-thinning by forming a three-dimensional network structure between particles. This network is formed by hydrogen bonding between the hydroxyl groups on the surface of fumed silica particles, which can trap the liquid and increase viscosity. As shear stress increases, this network begins to break down, allowing the material to flow more easily, which effectively lowers the n value. A lower n value indicates a stronger shear-thinning effect, which is beneficial in processes requiring high flowability under shear, such as DIW. Thus, FS enhances the processability of ceramic composites by promoting a more pronounced shear-thinning behavior, making the material easier to work with under applied

stress. Overall it appears that FS is a crucial for an inks rheology, these results will be checked again with our own ink formulas, Ink G and H, later on in the paper.

3.2.2 The Role of SiC on Rheological Properties (Ink D, E, and F)

Inks D, E, and F are all slurry formulations that were created for the purpose to help determine the role SiC plays in DIW slurries as it is added in various amounts. The first rheology test that these inks underwent was the steady rate sweep test to try and determine the viscoelastic behavior of the inks. On Figure 22, the thick black, red and blue lines represent Inks D, E, and F respectively, with the small red line running through each of the other lines representing each ink fitted to the Herschel-Bulkley model. The *n* value for Inks D, E, and F are 0.3, 0.7, and 1.2 respectively. From these *n* values it can be concluded that Inks D and E are suitable for DIW applications whereas Ink F is not suitable. From this, we conclude that as the amount of MK solution in the slurry increases, the ink will exhibit a higher *n* value.

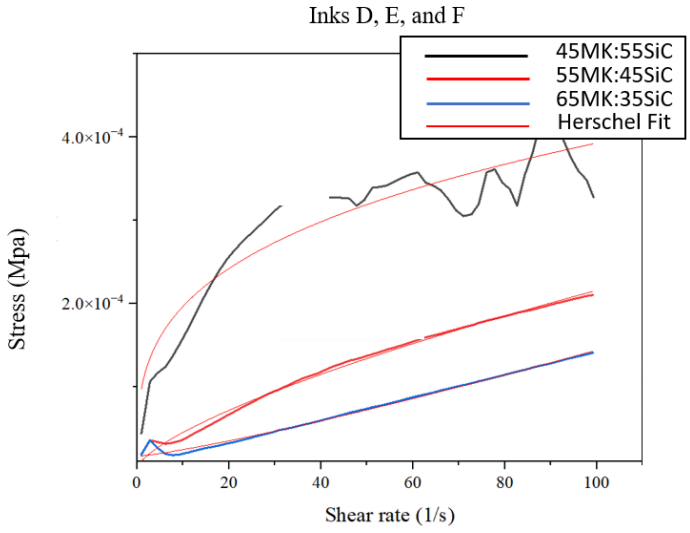

Figure 22 Steady Rate Seep Test of Inks D, E, and F with SiC

The next test conducted on Inks D, E, and F was the oscillation amplitude sweep test. Figures 23, 24, and 25 depict the results for Ink D, E, and F respectively. Inks D and E show the same results. The graph depicts, below G' and G" they never intersect indicating that these ink formula does not contain a crossover point. This is an indicator that these inks may not be suitable for DIW even though they contain shear thinning behavior. However, Figure 25, for Ink F does contain a crossover point. The intersection occurs at ~12% strain meaning that it falls into the low strain percentage category that is common in slurries for DIW. From this result it is possible to conclude that a high wt. % of SiC is needed for a crossover point to appear.

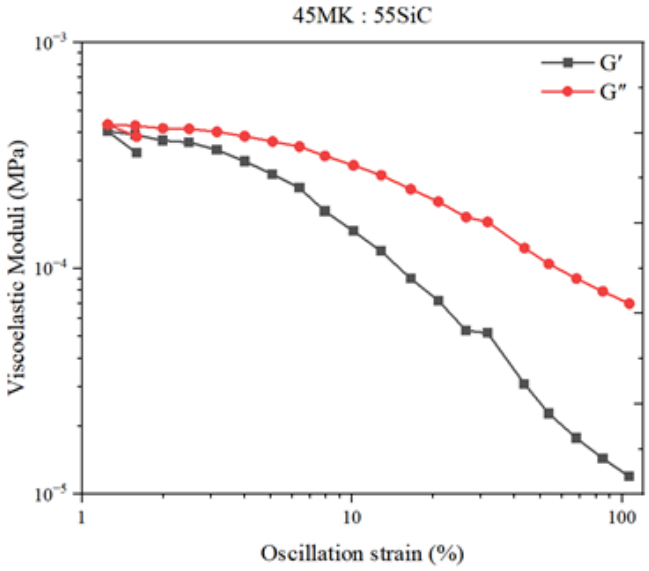

Figure 23 Oscillation Amplitude Sweep Test of Ink D

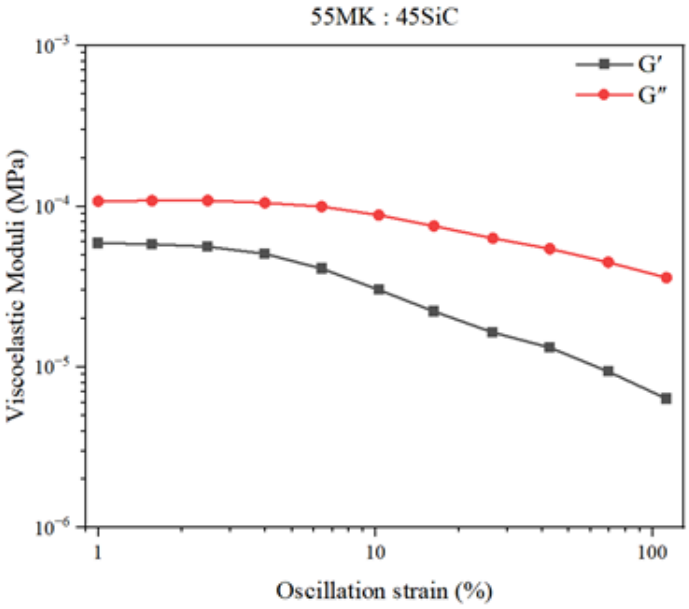

Figure 24 Oscillation Amplitude Sweep Test of Ink E

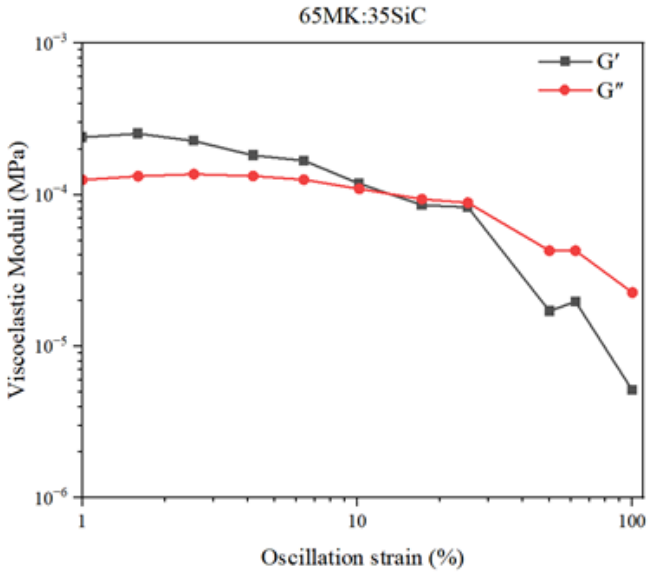

Figure 25 Oscillation Amplitude Sweep Test of Ink F

While Inks D, E, and F are not suitable for DIW applications a lot of conclusions can be drawn from the results. From the steady rate sweep test and the amplitude sweep test it can be

determined that the ideal amount of SiC that can be added is between 55 and 65 wt. %. This is because 65 wt. % failed the first test by exhibiting shear thickening behavior. However, this wt. % was able to successfully show a crossover point in the second test. The ink containing 55 wt. % of SiC was the exact opposite, exhibiting shear thinning behavior, but no crossover point. This means that an ideal wt. % of SiC to add exists between 55 and 65%.

The next inks to be tested, Inks G and H, were adapted from Inks D and F because they contained the highest disparity between *n* values. Ink D had the lowest *n* value displaying a more liquid-like tendency, and was less likely to be as impacted by shear forces as Ink E or F. In addition, Ink F was the only ink that had shown shear thickening behavior.

3.2.3 The Role of Fumed Silica on Rheological Properties (Ink G and H)

The first test inks G and H underwent was the steady rate sweep test with the results represented in Figure 26. The square-dotted black line and the circle-dotted red line represent Inks G and H respectively. The thin red line represents each ink fitted to the Herschel-Bulkley model. The purpose of this test was to determine the viscoelastic behavior of the inks after being modified with fumed silica. From analyzing the line, it was determined that the *n* value for Inks G and H are 0.17 and 0.86 respectively. By comparing these values to those found in the previous section (Ink D: n=0.3 and Ink F: n=1.2) it is noted that the *n* values decrease upon the addition of fumed silica. The *n* value from the ink with 45 wt. % MK solution decreases by 0.13 and the *n* value for the 65 wt. % MK solution decreases by 0.34. It might be then concluded that fumed silica has a greater impact on inks with greater solid-like viscoelastic properties.

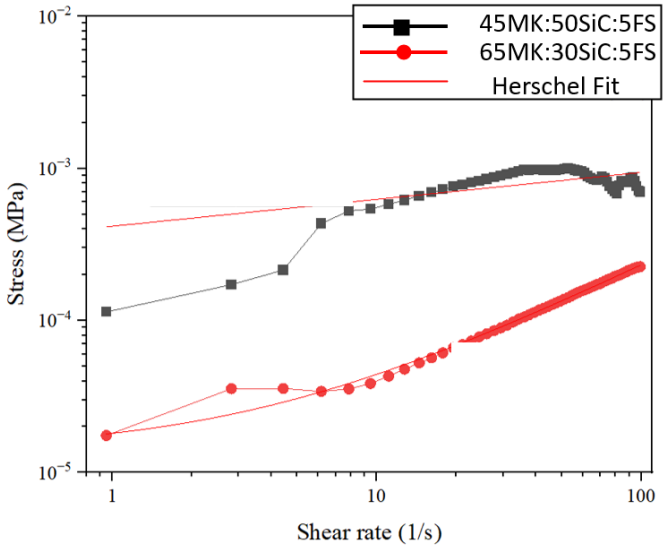

Figure 26 Steady Rate Sweep Test for Inks G and H with Fumed Silica

The next rheology test conducted was the oscillation amplitude sweep test to determine the crossover point in both Ink G and H, Figure 27 and 28 respectively. For Ink G, Figure 27, the graph shows that a crossover point now exists around ~1.5% strain. This is a significant improvement from Ink D's oscillation amplitude sweep graph which did not contain a crossover point. Ink H's crossover point appears to lower to around ~1% strain when compared to the original 12% strain seen in Ink F. From these results and the previous results from Inks A and B it is possible to conclude that fumed silica has an overall positive effect on an inks crossover point.

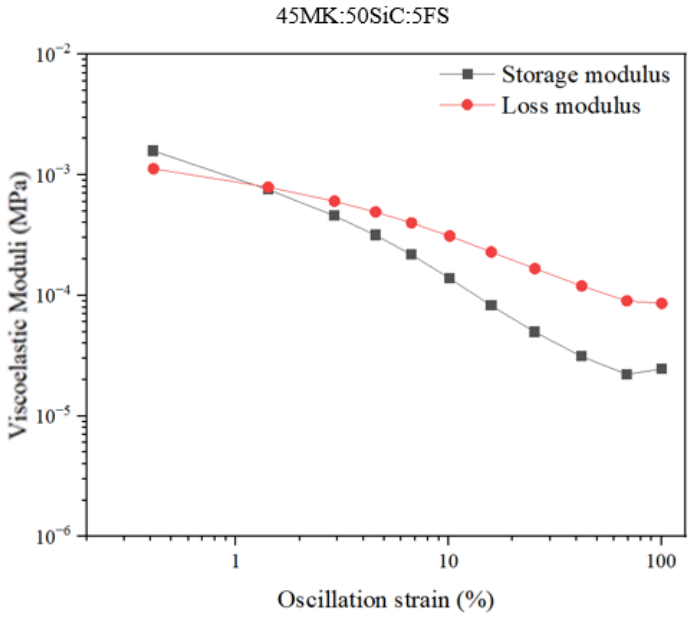

Figure 27 Oscillation Amplitude Sweep Test of Ink G

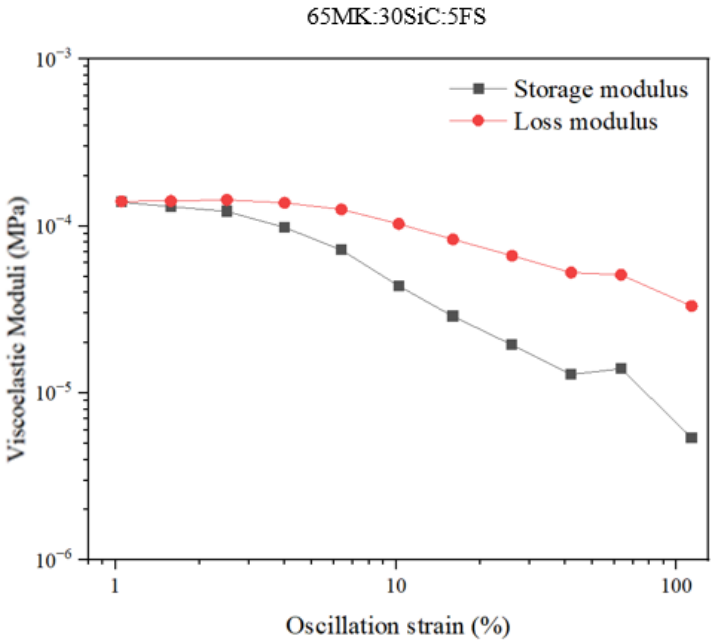

Figure 28 Oscillation Amplitude Sweep Test of Ink H

Comparing the steady rate sweep results of Ink D with Ink G it is seen that the addition of FS

leads to a decrease in the *n* value, the same can be seen when comparing the results from Inks F and H. This means that FS is improving the flowability of the ink allowing the ink to achieve shear thinning behavior more easily, especially if there is already a high solid content present. In SiC-based ceramic slurries, FS particles contribute to shear-thinning by forming a three-dimensional network structure between particles. This network is formed by hydrogen bonding between the hydroxyl groups on the surface of fumed silica particles, which can trap the liquid and increase viscosity. As shear stress increases, this network begins to break down, allowing the material to flow more easily, which effectively lowers the n value. A lower n value indicates a stronger shear-thinning effect, which is beneficial in processes requiring high flowability under shear, such as DIW. Thus, FS enhances the processability of ceramic composites by promoting a more pronounced shear-thinning behavior, making the material easier to work with under applied stress.

Comparing the amplitude sweep tests results of Ink D with Ink G it is seen that the addition of FS leads to the formation of a crossover point as one was not previously observed in Ink D's results. Then the steady rate sweep results of Ink F with Ink H, it can be seen that the addition of fumed silica decreased the value of the crossover point. This is a contradiction as it appears that FS does not help Ink H with flow behavior, while it does help Ink G and Ink A. This contradiction can be ruled as an outlier due to the high solid content within the ink formula.

3.2.4 The Role of Carbon Fibers on Rheological Properties (Ink I, J, and K)

The first test inks I, J, and K underwent was the steady rate sweep test represented in Figure 29. The black, blue, and pink lines represent Ink I, J, and K respectively. The thin red line represents the data fitted to the Herschel-Bulkley model for Ink I, resulting in an *n* value of 0.25. It became

difficult to find the *n* values for Inks J and K because of the shape of the line. The reason Inks J and K could not be modeled by the Herschel bulkily model could be because the shape of the graph is more of a parabolic shape, and going down faster than anticipated. Another reason could be that the rheometer is having a difficult time producing results on account of the randomized fibers causing higher than normal stress values. As seen in the previous samples in this study the shear stress has been in the order of 10^{-4}, however these results are in the order of 10^{-3}.

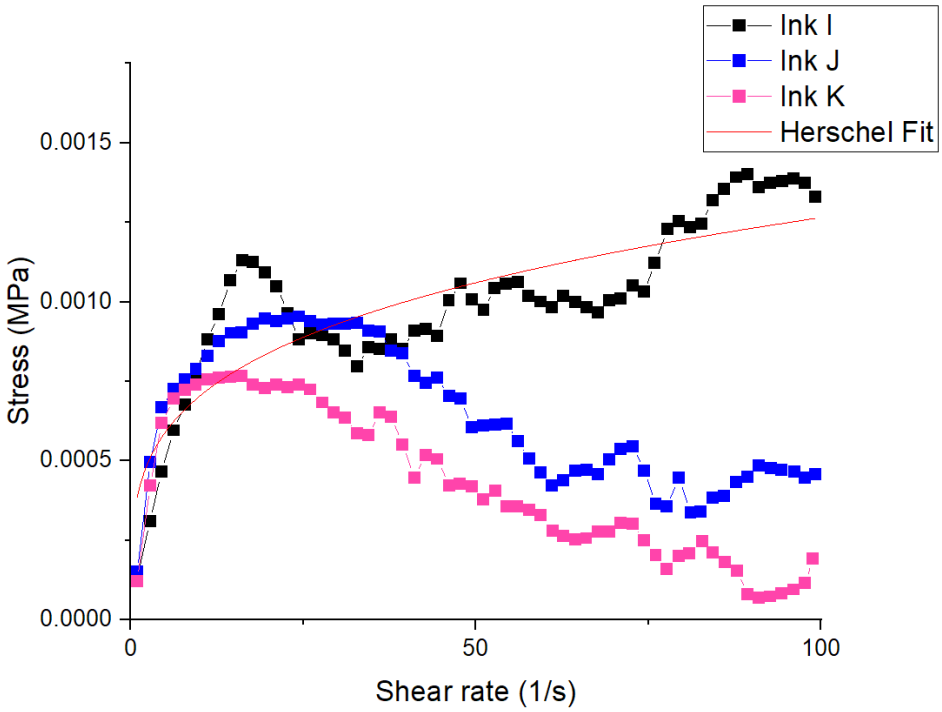

Figure 29 Steady State Rate Sweep Test for Inks I, J, and K with C_f

The next rheology test conducted was the oscillation amplitude sweep test to determine the crossover point in Inks I, J, and K, Figure 30, 31, and 32 respectively. For Ink I, the crossover point does not last long, only extending to ~0.3% strain. And while a low crossover point is needed for DIW applications, one this low makes Ink I potentially not suitable for DIW. For Inks J and K, the crossover point lasts longer than that of Ink I, extending to ~2% strain. While this

region is on the smaller end, it still makes these inks more suitable for DIW applications than Ink I.

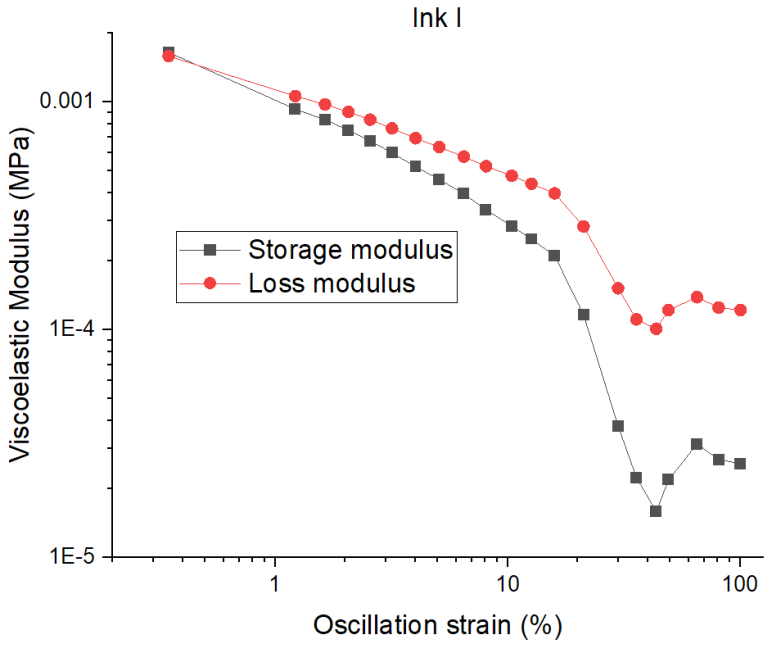

Figure 30 Oscillation Amplitude Sweep Test of Ink I

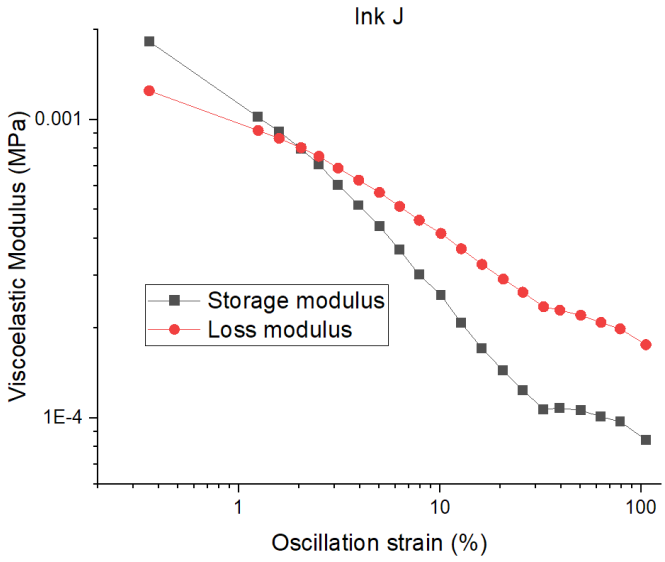

Figure 31 Oscillation Amplitude Sweep Test of Ink J

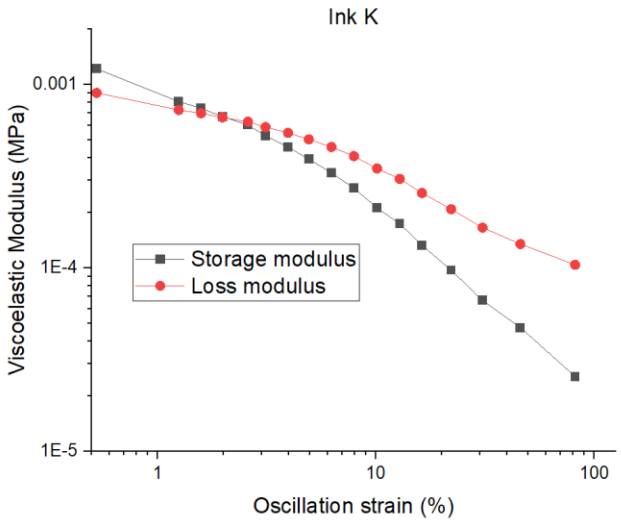

Figure 32 Oscillation Amplitude Sweep Test of Ink K

From the steady rate sweep test of Inks, I, J, and K it is not possible to draw any conclusions about carbon fiber's impact on the overall flow behavior of the ink. Then when analyzing the results of the results of the amplitude sweep test it can be seen that increasing the amount of C_f within an ink formula can marginally improve the crossover point, meaning the ink's structure in terms of rheology is improving as more C_f is added.

3.3 Pyrolysis and Microstructure Characterization

3.3.1 Thermo-gravitational Analysis (TGA) Test

To understand the phase transformation during the pyrolysis, we performed a thermo-gravitational (TGA) test was conducted on Ink A to determine a temperature where the most amount of mass was being lost in the sample.

The test was performed in an air environment where the test started at room temperature (~20℃) and increased at a rate of 10 ℃/min minute until a temperature of 1100 ℃ was reached. The goal was to find the temperature ranges where the greatest mass loss occurs is to create a two-step pyrolysis process where the sample is held at the found temperature and then continues to the max temperature. Figure 33 below shows the results of the TGA test comparing the mass loss in milligrams (mg) to temperature (°C). Analyzing the graph, the temperature ranges with mass loss can be found between 500℃ and 600℃ and the second is between 700℃ and 900℃. Based on this graph an initial pyrolysis temperature of 900℃ was determined to be an ideal starting point.

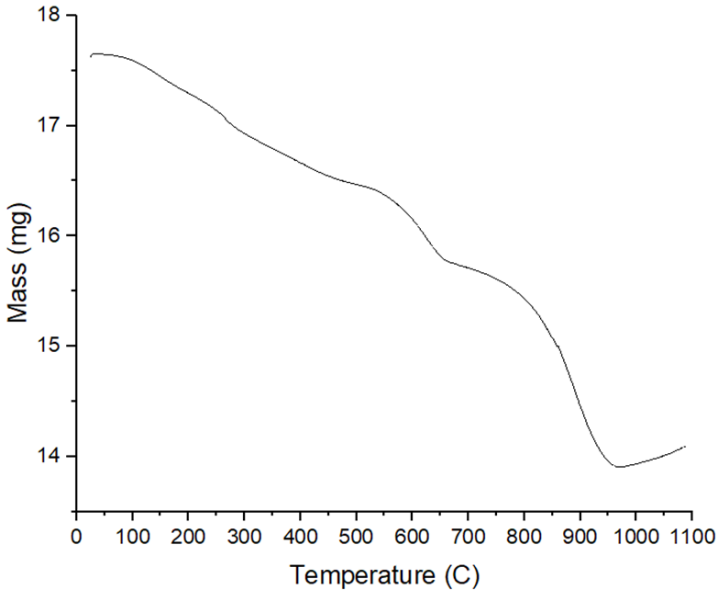

Figure 33 Thermo-gravitational graph of Ink A, recording mass loss in comparison with time.

The samples were loaded into the Sentro 1800 ℃ furnace to undergo the process of pyrolysis. This process was conducted within an air environment, with a focus on three main parameters: max temperature, temperature ramp rate, and dwell time. The dwell time is the only parameter

that remained constant for one hour. The other two parameters were modified based on the results of previous tests. The first test described in Table 6 used Inks A and B whose formulas contained all the additives to serve as a base line for the other ink samples. Temperature and ramp rate of these first tests were decided based primarily on the TGA graph discussed in the above section, they were also based on prior research that had been done on the fast pyrolysis of ceramics and are presented in table 6 [36, 37].

Table 6 Pyrolysis Testing Overview

Ink	Max Temperature (°C)	Ramp Rate (°C/min)	Dwell Time (Hour)	Environment
A&B	900	3.5	1	Air
All Samples (A-K)	1300	1	1	Air
All Samples (A-K)	1000	1	1	Air
K	800	10	1	Air
K	800	20	1	Air

After the samples were retrieved from the furnace, they were analyzed noting any changes such as color change, surface changes, and size changes. Further micro analysis was possible on these samples with the SEM machine analyzing things such as: pore size/density, fibers, fiber alignment, cracks, and any surface defects.

After the samples were removed from the furnace, they are taken to the scanning electron microscope (SEM) to be characterized. The characterization of samples consisted of analyzing the porosity, surface quality, fiber alignment, and particle adhesion. The analysis of the surface quality was done by carefully breaking off a roughly 4-5 mm segment of the sample.

3.3.2 Pyrolysis of Reference Inks (A&B) for Tests 1, 2, and 3 (900, 1300, and 1000 ℃)

3.3.2.1 Test 1 – 900 ℃

Ink samples A and B were the two specimens initially subjected to pyrolysis treatment as part of this study. The pyrolysis of Inks A and B, was conducted under the specific parameters outlined in Table 7 with results illustrated in Figures 34 a, b, and 35 a, b, and c for Ink A, and Figures 36 a and b and 37 a, b, and c for Ink B. These figures provide visual insights into the shrinkage and structural changes experienced by each sample.

Figure 34a and b show Ink A before pyrolysis and after pyrolysis, respectively, and by comparing these two images it can be observed that Ink A underwent an overall linear shrinkage of 20.844 mm or 3.18%. This level of shrinkage is consistent with the expected dimensional changes typically observed in SiC ceramic parts during pyrolysis. The controlled shrinkage observed in this sample suggests that the pyrolysis treatment was effective in maintaining the structural integrity of the ceramic while reducing its size within anticipated limits. It can also be observed that a color change took place before and after pyrolysis, a clear sign of a chemical change proving that a ceramic was formed. This color change indicates that the preceramic polymer used in the study was successfully converted into a SiC ceramic. After analyzing the outward appearance of Ink A, the next step is analyzing the Ink was to us an SEM machine. Figure 35a shows an image of the surface of Ink A at 250x magnification and 100µm scale. Surface view shows the large number of cracks present which is a clear indication of either thermal stress or a chemical imbalance. Figure 35b indicates the pore and layered granular present in the cross-section of Ink A, at 40x magnification and 500µm scale. These results are an indicator that the ceramic was only partially formed upon pyrolysis. At higher magnification,

1,500x magnification and 10µm scale, Figure 35c depicts the small holes with carbon fiber strands like the prior inks results. Yet an important observation is that many of the carbon fiber holes were aligned in the same print direction, the print direction. Showing that the shear stress created by the nozzle is sufficient to re-align the fibers in a uniform direction. Seeing the fibers align also shows that Ink A has sufficient rheological properties to keep the fibers from re-orienting themselves once the Ink leaves the nozzle.

Table 7 Pyrolysis Parameters for Test 1

Ink	Max Temperature (℃)	Ramp Rate (℃/min)	Dwell Time (Hour)	Environment
A&B	900	3.5	1	Air

Figure 34a and b Pyrolysis of Ink A (a) before and (b) after pyrolysis at 900 ℃, 3.5 ℃/min, and 1 hour dwell time.

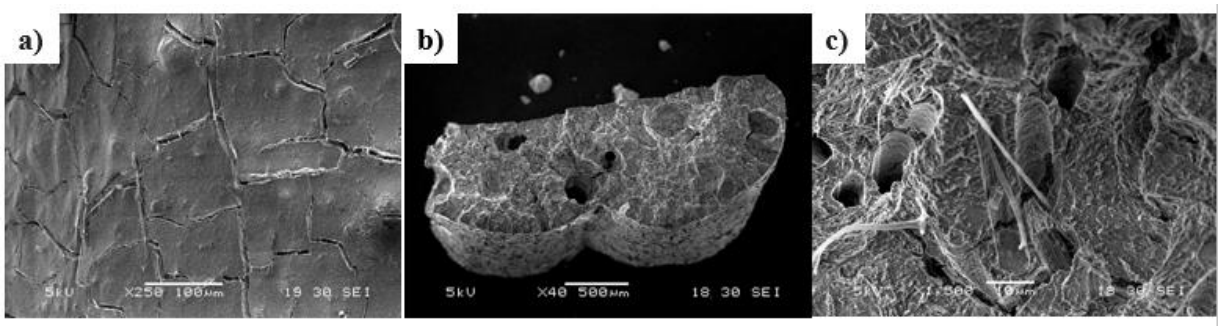

Figure 35 a, b, and c SEM images of Ink A at 900 ℃, 3.5 ℃/min, and 1 hour dwell time. (a) Surface image at 250x magnification and 100µm scale. (b) Broad cross-sectional image taken at 40x magnification and 500µm scale. (c) close-up cross-sectional image taken at 1500x magnification and 10µm scale.

Ink B's before and after pyrolysis results are shown in Figure 36a and b. Comparison of these two images results in the observation that Ink B underwent an overall linear shrinkage of 25.169 mm or 3.84%. This level of shrinkage is consistent with the expected dimensional changes typically observed in SiC ceramic parts during pyrolysis. The controlled shrinkage observed in this sample suggests that the pyrolysis treatment was effective in maintaining the structural integrity of the ceramic while reducing its size within anticipated limits. It can also be observed that a color (chemical) change took place before and after pyrolysis, just like with Ink A for a successful conversion into a SiC ceramic. After analyzing the outward appearance of Ink B, analysis with the SEM machine. Figure 37a, shows an image of the surface of Ink B at 250x magnification and 100µm scale. With cracks present, it is clear a thermal stress or chemical imbalance occurred. Figure 37b a cross-sectional image of Ink B, at 40x magnification and 500µm scale shows the size and number of the pores along with the presence of a smooth structure in the cross-section. This smooth structure, which is not present in Ink A, is an

indication that the ceramic structure had more success in forming in Ink B than Ink A. This change in structure is believed to be caused by the presence of fumed silica. Figure 37c shows the same small holes of the size of the milled carbon fibers but less of them indicating that the fumed silica presence is helpful in binding the fibers more closely to the ceramic matrix. Since the fibers are also aligned, Ink B has sufficient rheological properties to keep the fibers from re-orienting themselves once the Ink leaves the nozzle. Yet since there was the creation of some indents parallel to the cross-section, it is believed that the shear stress produced by the nozzle is not high enough for the fibers to align properly or there may not be enough solid wt.% in the Ink formulation.

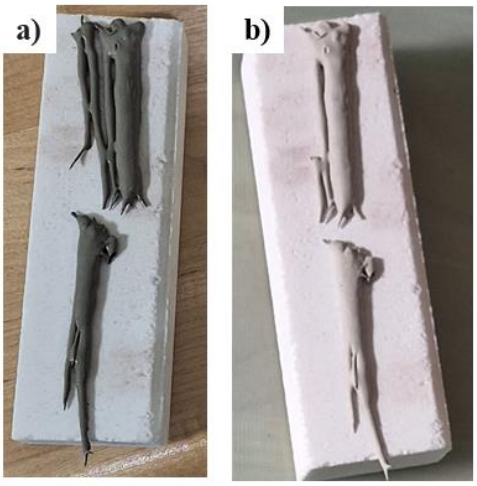

Figure 36a and b Pyrolysis of Ink B (a) before and (b) after pyrolysis at 900 ℃, 3.5 ℃/min, and 1 hour dwell time.

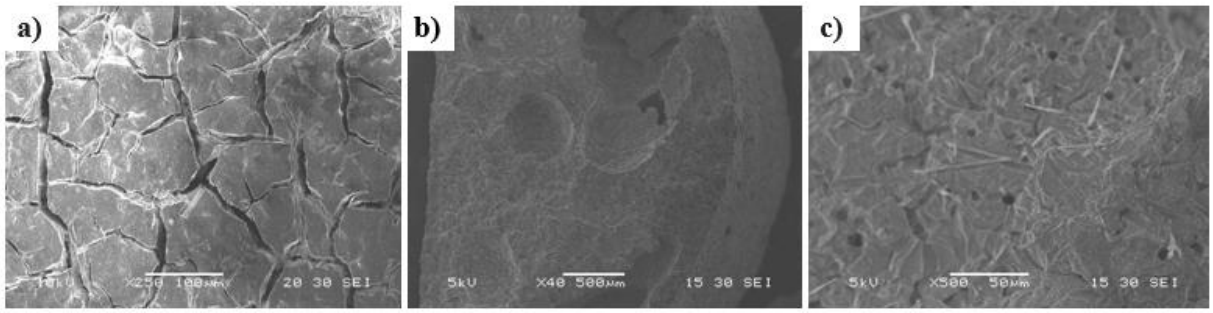

Figure 37a, b, and c SEM images of Ink B at 900 ℃, 3.5 ℃/min, and 1 hour dwell time. (a) Surface image at 250x magnification and 100µm scale. (b) Broad cross-sectional image taken at 40x magnification and 500µm scale. (c) close-up cross-sectional image taken at 500x magnification and 50µm scale.

3.3.2.2 Test 2 – 1300 ℃

The pyrolysis of Inks A and B, was conducted under the specific parameters outlined in Table 8 with the results illustrated in Figures 38 a and b and Figures 39 a, b, and c for Ink A, and Figures 40 a and b and Figures 41 a, b, and c for Ink B. These figures provide visual insights into the shrinkage and structural changes experienced by each sample.

Figure 38a and b show Ink A before pyrolysis and after pyrolysis, respectively with an overall linear shrinkage of 6.613 mm or 12.69%. which is consistent with the expected dimensional and color change typically observed in SiC ceramic parts during pyrolysis. Analysis with the SEM machine as shown in Figure 39a showing the surface at 100x magnification and 100µm scale shows continued thermal or chemical imbalance presence because of the cracking present. Since the fibers are aligned in the print direction on the surface, there is a high probability they are aligned in the cross-section as well and that is seen in Figure 39b showing a cross section at 85x magnification and 200µm scale. Like a prior test, there are still pores present but unlike the

previous pyrolysis test conducted at 900 ℃, this sample had a smooth cross-section surface structure meaning that the ceramic structure was fully formed. Figure 39c shows an image of the cross-section of Ink A at a higher magnification, 500x magnification and 50µm scale. In this last image it is important to note the small holes are the exact size of the milled carbon fibers used and while still everywhere, there were no strands/remnants of carbon fiber indicating the temperature was too high and caused complete oxidization before the SiC matrix had been fully formed. But all the fibers remain in the same print direction, so the formula still holds to extrusion from the ink nozzle.

Table 8 Pyrolysis Parameters for Test 2

Ink	Max Temperature (℃)	Ramp Rate (℃/min)	Dwell Time (Hour)	Environment
All Samples (A-K)	1300	1	1	Air

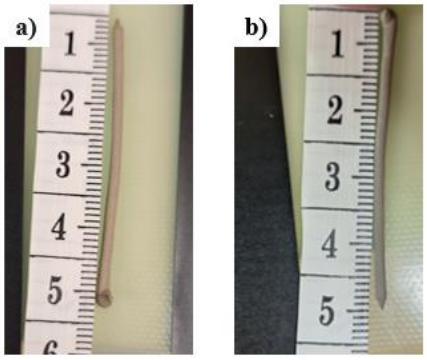

Figure 38a and b Pyrolysis of Ink A (a) before and (b) after pyrolysis at 1300 ℃, 1 ℃/min, 1 hour

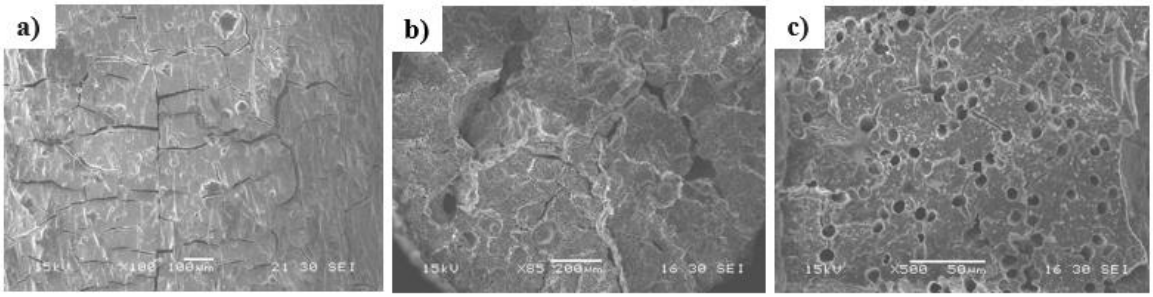

Figure 39a, b, and c SEM images of Ink A at 1300 ℃, 1 ℃/min, and 1 hour dwell time. (a) Surface image at 100x magnification and 100µm scale. (b) Broad cross-sectional image taken at 85x magnification and 200µm scale. (c) close-up cross-sectional image taken at 500x magnification and 50µm scale.

Figure 40a and b show Ink B before pyrolysis and after pyrolysis, respectively. Ink B failed under the pyrolysis conditions depicted in Table 8. The sample had completely adhered to the furnace block indicating that fumed silica may be helping the ink to survive at higher processing temperatures. Scrapping off the remnants from Ink B the outward appearance of the sample showed a clear color change took indicating a successful conversion into a SiC ceramic. Analysis with an SEM machine at 200x magnification and 100µm scale is seen in Figure 41a. Cracks are present and more severe than those of Ink A further supporting the hypothesis that fumed silica helps the ceramic survive at higher pyrolysis temperature. Figure 41b shows an image of the cross-section of Ink B at 200x magnification and 100µm scale and like Ink A all the carbon fiber had been oxidized. Other than the observation of the carbon fiber no longer being visible, there are no other observations to be made about Ink B as the cross-section was too damaged for further observations so no conclusions can be made about the direction of the fibers in relation to the printing direction.

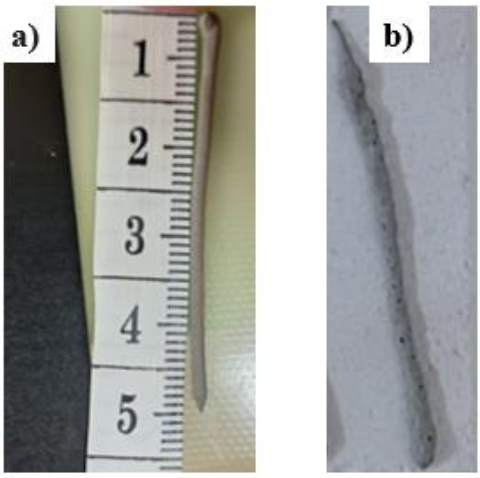

Figure 40a and b Pyrolysis of Ink B (a) before and (b) after pyrolysis at 1300 ℃, 1 ℃/min, and 1 hour dwell time.

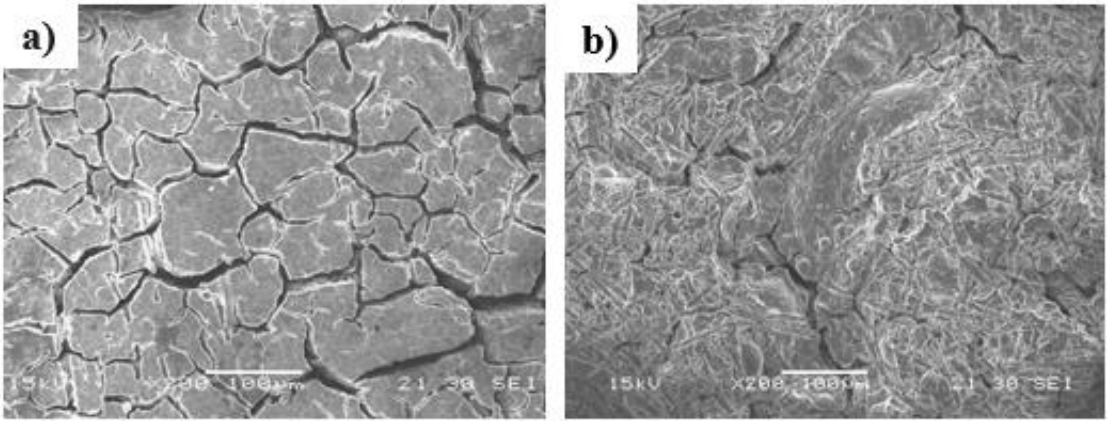

Figure 41a and b SEM images of Ink B at 1300 ℃, 1 ℃/min, and 1 hour dwell time. (a) Surface image at 200x magnification and 100µm scale. (b) Broad cross-sectional image taken at 200x magnification and 100µm scale.

3.3.2.3 Test 3 – 1000 ℃

Pyrolysis of Inks A and B, was conducted under altered parameters outlined in Table 9 with results illustrated in Figures 42 a and b, Figures 43 a, b, and c, and Figure 44 for Ink A. Figures

45 a and b and 46 a b and c represent Ink B. These figures provide visual insights into the shrinkage and structural changes experienced by each sample. Figure 42a and b show Ink A before and after pyrolysis respectively. By comparing these two images it can be observed that Ink A underwent an overall linear shrinkage of 3.514mm or 10.76%. It should be noted that the sample shown in Figure 42b is in three fragments, this is due to the fragility of the sample and improper handling. The sample broke after being extracted from the furnace and did not break during pyrolysis. A shrinkage of 10.76% is consistent with the expected dimensional changes typically observed in SiC ceramic parts during pyrolysis. The controlled shrinkage observed in this sample suggests that the pyrolysis treatment was effective in maintaining the structural integrity of the ceramic while reducing its size within anticipated limits. It can also be observed that while a color change took place, it was less pronounced than the color change seen in Ink A in test 1, and more closely matched that of Ink A in test 2. This indicates that the ceramic matrix seems to form between 900℃ and 1300℃. Analyzing the ink using the SEM machine, Figure 43a shows it is possible to view some strands of fiber on the surface and that they are aligned in the print direction on the surface for which because of this it is believed that there is a high probability they fibers were aligned in the cross-section as well. Figure 43b shows an image of the cross-section of Ink A at 60x magnification and 200µm scale. From the broad view of the cross-section there were two things that stood out and they were the size and number of the pores and the smooth structure present in the cross-section. Unlike the previous pyrolysis test conducted at 900 ℃, this sample had a smooth cross-section surface structure meaning that the ceramic structure was fully formed. Figure 43c shows an image of the cross-section of Ink A at a higher magnification, at 650x magnification and 20µm scale. In this last image it is important to note the small holes that seem to be everywhere in the cross-section. These holes, upon

measuring them, were found to be the exact size of the milled carbon fibers used in the ink. Small fiber remnants can be seen as highlighted by the yellow circles in Figure 44. Seeing these remnants indicates that most carbon fibers are still oxidizing, but some remnants are still intact. Much like the results from test 1. Another important observation while examining the cross-section is that many of the carbon fiber holes are all aligned in the same direction, the print direction. This is an important observation because it means that the shear stress created by the nozzle is sufficient to re-align the fibers in a uniform direction. Seeing the fibers align like this also shows that Ink A has sufficient rheological properties to keep the fibers from re-orienting themselves once the Ink leaves the nozzle.

Table 9 Pyrolysis Parameters for Test 3

Ink	Max Temperature (℃)	Ramp Rate (℃/min)	Dwell Time (Hour)	Environment
All Samples (A-K)	1000	1	1	Air

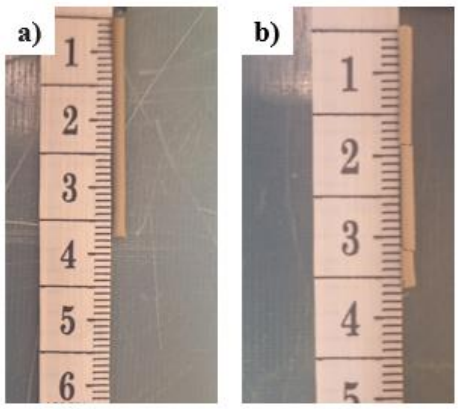

Figure 42a and b Pyrolysis of Ink A (a) before and (b) after pyrolysis at 1000 ℃, 1 ℃/min, and 1 hour dwell time.

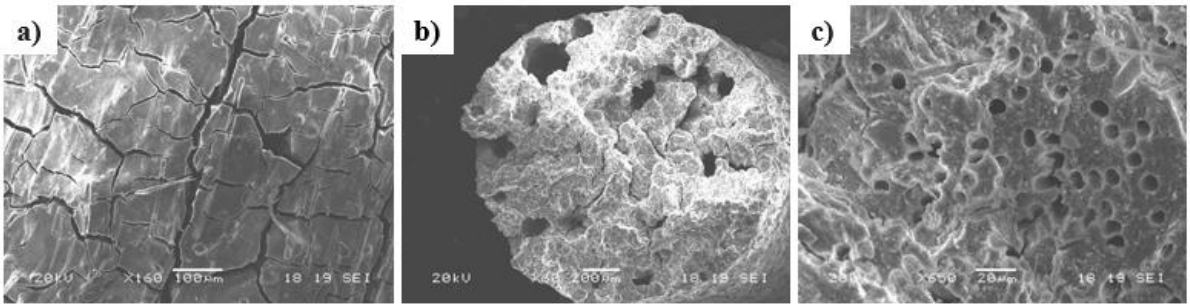

Figure 43a, b, and c SEM images of Ink A at 1000 ℃, 1 ℃/min, and 1 hour dwell time. (a) Surface image at 160x magnification and 100µm scale. (b) Broad cross-sectional image taken at 60x magnification and 200µm scale. (c) close-up cross-sectional image at 650x magnification and 20µm scale.

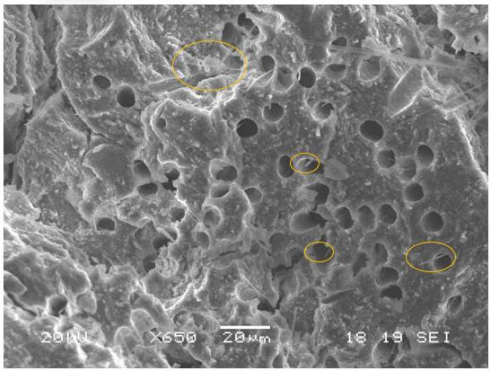

Figure 44 Ink A SEM cross-sectional image of fiber holes taken at 650x magnification and 20µm scale. Yellow circles highlight the remnants of the carbon fiber remaining after pyrolysis.

Figure 45a and b show Ink B before pyrolysis and after pyrolysis respectively. Ink B failed under these pyrolysis conditions depicted in Table 12. Ink B failed in such a way that the sample had completely adhered to the furnace block the sample was placed on. This indicates that fumed silica may be helping the inks to survive at higher processing temperatures. By carefully scrapping off Ink B from the furnace block, it was possible to perform SEM imaging on the parts

that were scraped off. It was also be observed that a color change took place before and after pyrolysis, just like Ink A, a clear sign of a chemical change. The degree of color change is much like that seen in Ink A, indicating that the ceramic structure forms somewhere between 900℃ and 1300℃. This color change means that the preceramic polymer used in this study was successfully converted into a SiC ceramic. After analyzing the outward appearance of Ink B, the next step was analyzing the ink using the SEM machine. Figure 46a shows an image of the surface of Ink B, at 50x magnification and 500µm scale. From looking at the surface the most noticeable thing is the number of cracks that are present, a clear indication of some type of thermal stress or chemical imbalance within the ceramic matrix composites. Figure 46b shows an image of the cross-section of Ink B, at 50x magnification and 500µm scale. From the broad view of the cross-section there were two things that stood out and they were the size and number of the pores, and the smooth structure present in the cross-section. Figure 46c shows an image of the cross-section of Ink B at a higher magnification, at 220x magnification and 100µm scale. In this last image as like prior ink formulations, there are many small holes that were found to be the exact size of the milled carbon fibers used in the ink. However, there are little to no fiber strands found in Ink B's cross-section, which is an indication that fumed silica is helping to bound the fibers more closely to the ceramic matrix. Ink B also has indents in the print direction indicating it has sufficient rheological properties to keep the fibers from re-orienting themselves once the Ink leaves the nozzle.

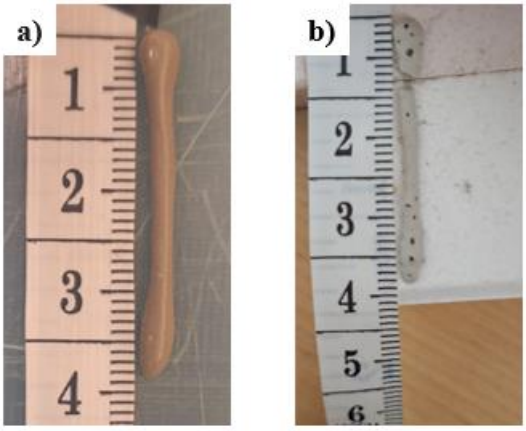

Figure 45a and b Pyrolysis of Ink B (a) before and (b) after pyrolysis at 1000 ℃, 1 ℃/min, and 1 hour dwell time.

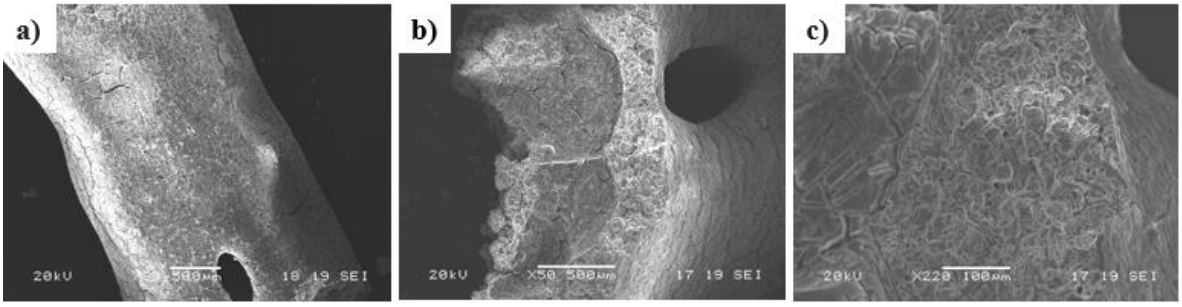

Figure 46a, b, and c SEM images of Ink B at 1000 ℃, 1 ℃/min, and 1 hour dwell time. (a) Surface image at 50x magnification and 500µm scale. (b) Broad cross-sectional image taken at 50x magnification and 500µm scale. (c) close-up cross-sectional image taken at 220x magnification and 100µm scale.

3.3.2.4 Conclusions about the effect of FS based on Reference Inks

The results from these pyrolysis parameters seem to indicate that fumed silica helps to more closely bind the structure but may require a higher processing temperature for the ceramic to fully form. Based on this indication, the next test was conducted at a higher processing

temperature and a slower ramp rate to allow the ceramic matrix to fully form. Ink B had consistently failed throughout test 2 and 3, indicating that Ink B is not ideal for DIW, and this is backed up by the rheology results that Ink B experiences shear thickening. However, Ink B also contains a crossover point, which is another significant rheology property as it helps indicate if the structure is stable. This seems to point to the conclusion that the flow behavior of the ink is significantly more important to study than the crossover point. Another important result to note of is the lack of carbon fibers visible throughout both inks, and all tests. This lack of fiber visibility appears to point to the conclusion that all of the fibers had oxidized during pyrolysis.

3.3.3 Role of Silicon Carbide (SiC) based of Inks D, E, and F at 1300 ℃ and 1000 ℃

3.3.3.1 Test 2 Inks D, E, and F at 1300 ℃

Inks D, E, and F were the next samples to undergo pyrolysis. The parameters are outlined in Table 8 and results illustrated in Figures 47 a and b, Figures 48 a and b, and Figure 49 for Ink D, Figures 50 a and b and Figure 51 for Ink E, and Figures 52 a and b for Ink F. These figures provide visual insights into the shrinkage and structural changes experienced by each sample. As seen in the before and after, Figure 47 a and b respectively, Ink D underwent a color change to indicate a ceramic was formed and an overall linear shrinkage of 6.225 mm or 11.4% was observed which is consistent with the expected dimensional changes typically observed in SiC ceramic parts during pyrolysis. The difference in outcomes is the presence of large air bubbles which while a sign of a chemical reaction, does indicate a reaction of a negative type. This was most likely caused by thermal expansion of air within the pores of the sample seen in figure 48a. Figure 48b, an image of the cross-section of Ink D, at 55x magnification and 200μm scale shows

the same smooth structure as is in Ink A and B for a fully formed ceramic output. The cracks seen in the resulting product are much less severe than those seen in samples with more additives. It is theorized from this that adding more additives, increases the thermal stress put onto the sample. The sample also has large pores as seen more closely in Figure 49 along with long cracks on the inside walls an indication that air forced its way out.

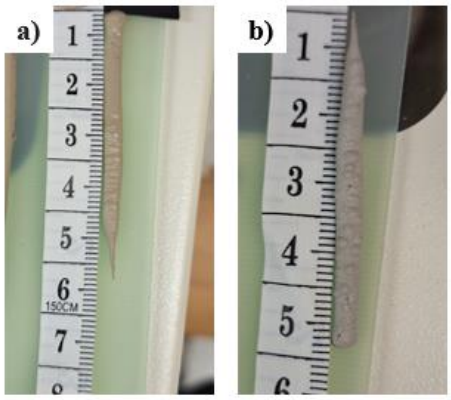

Figure 47a and b Pyrolysis of Ink D (a) before and (b) after pyrolysis at 1300 ℃, 1 ℃/min, and 1 hour dwell time.

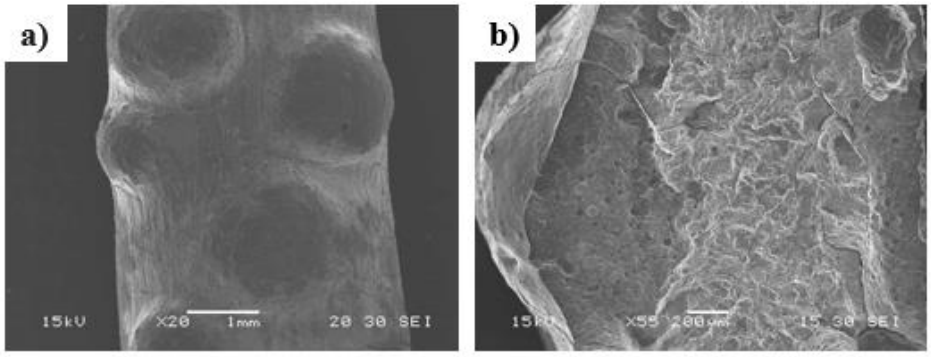

Figure 48a and b SEM images of Ink D at 1300 ℃, 1 ℃/min, and 1 hour dwell time. (a) Surface image at 20x magnification and 1mm scale. (b) Broad cross-sectional image taken at 55x magnification and 200µm scale.

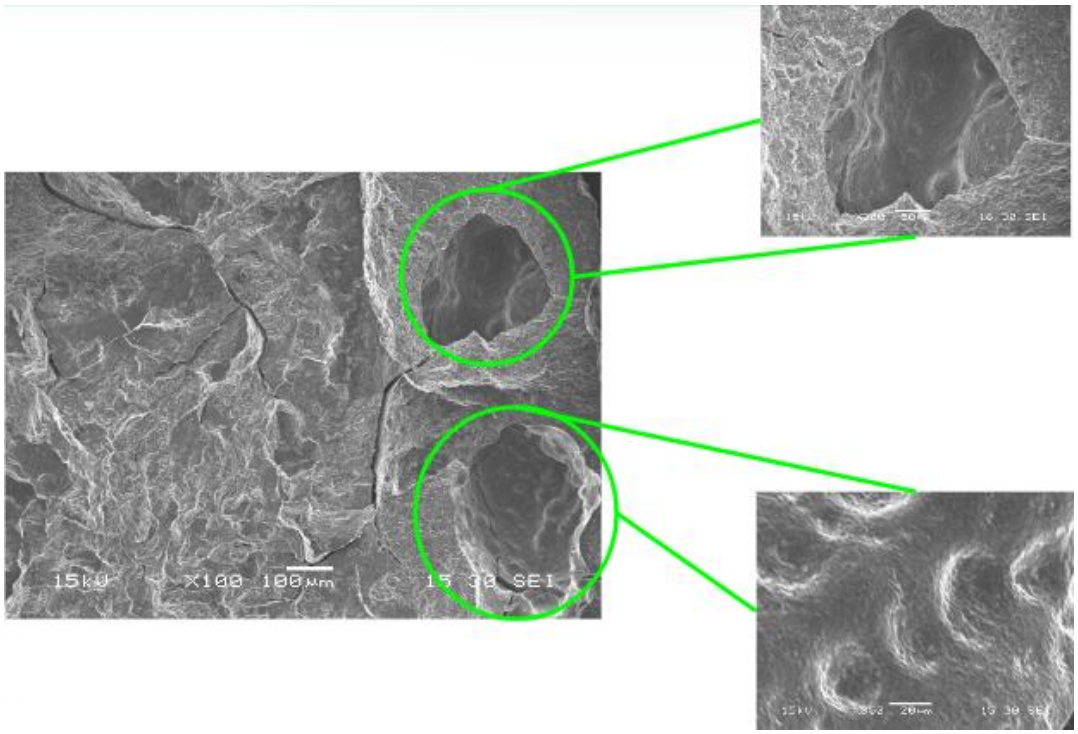

Figure 49 In depth view of cross-sectional features depicting a closer look at a pore and the structure.

Ink E's results from before and after pyrolysis are shown in Figure 50a and b, respectively showing Ink E failed under the pyrolysis conditions depicted in Table 8. As with Ink B, Ink E had completely failed and adhered to the furnace block. Resulting in a hypothesis that an increased amount of MK solution results in a greater possibility of failure upon pyrolysis. A small sample was obtained to perform SEM imaging shown in Figure 51, a cross-section of Ink E, at 50x magnification and 500µm scale. From the broad view of the cross-section, it could be seen that the while the sample does have a smooth surface there are too many cracks and pores to

draw any more conclusions about the effect of SiC on this sample.

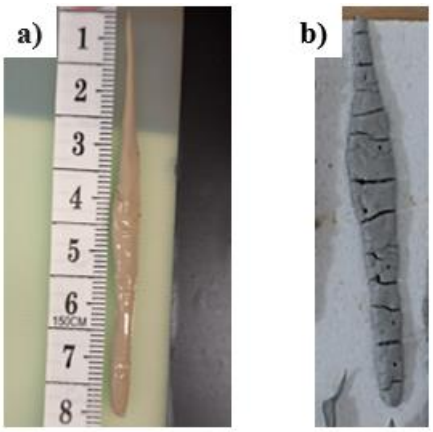

Figure 50a and b Pyrolysis of Ink E (a) before and (b) after pyrolysis at 1300 ℃, 1 ℃/min, and 1 hour dwell time.

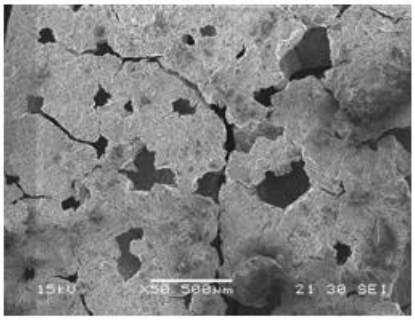

Figure 51 SEM images of Ink E at 1300 ℃, 1 ℃/min, and 1 hour dwell time. Depicting the surface image at 50x magnification and 500µm scale.

Ink F similarly failed as depicted in Figure 52a and b which show Ink F before and after pyrolysis and after pyrolysis, respectively. Giving the indication that by increasing the amount of MK solution present in the Ink, there is a greater possibility of failure upon pyrolysis. This further supports the outcome that as less SiC is added, the more likely the sample is to fail. Unlike Inks B and F no sample fragments were able to be retrieved to perform SEM imaging.

However, the outward appearance indicated a color change so that the preceramic polymer used in the study was successfully converted into a SiC ceramic.

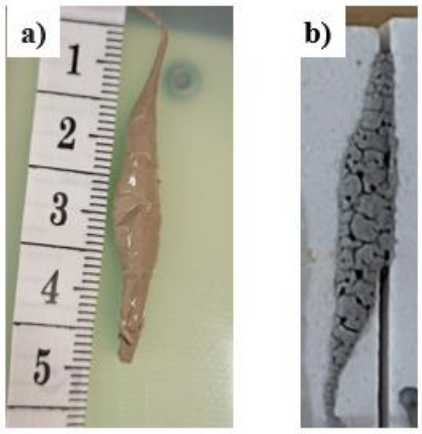

Figure 52a and b Pyrolysis of Ink F (a) before and (b) after pyrolysis at 1300 ℃, 1 ℃/min, and 1 hour dwell time.

3.3.3.2 Test 3 Inks D, E, and F at 1000 ℃

Inks D, E, and F were the next samples to undergo pyrolysis with the new parameters outlined in Table 9. The pyrolysis results for Inks D, E, and F are illustrated in Figures 53 a and b and Figures 54 a, b, and c for Ink D, Figures 55 a and b and Figures 56 a and b for Ink E, and Figures 57a and b for Ink F. Figure 53a and b show Ink D before and after pyrolysis with an overall linear shrinkage of 0.888 mm or 1.58%. This is consistent with the expected dimensional changes typically observed in SiC ceramic parts during pyrolysis. It was also be observed that a color change took place before and after pyrolysis for proof that a ceramic was formed. And therefore, like most other inks, the preceramic polymer used in this study was successfully converted into a SiC ceramic. It should also be noted that there are no large bubbles on the surface as seen in Test 2 of Ink D. Figure 54a shows an image of the surface of Ink D, at 25x

magnification and 1mm scale using the SEM. The most noticeable surface feature on Ink D are the large and numerous cracks running along the surface of the part. These cracks are a clear indication of thermal stress, which means that the processing temperature was too high. Figure 54b shows an image of the cross-section of Ink D, at 40x magnification and 500µm scale. From the broad view of the cross-section the sample is seen to have a relatively smooth surface quality. However, there appear to be two very large pores and several small cracks on the cross-section's surface. These cracks are much less severe than those seen in samples with more additives, leading to a theory that by adding more additives, it increases the thermal stress put onto the sample. Figure 54c shows a close-up image of the cross-section of Ink D, at 3000x magnification and 5µm scale. This very close-up image seems to contradict the conclusion drawn from the broad cross-sectional image. This is because the close-up image when magnified looks granular at this level of magnification for ceramics. The important observation to take away is that the grains are bonded together properly and there are no partial bonds visible.

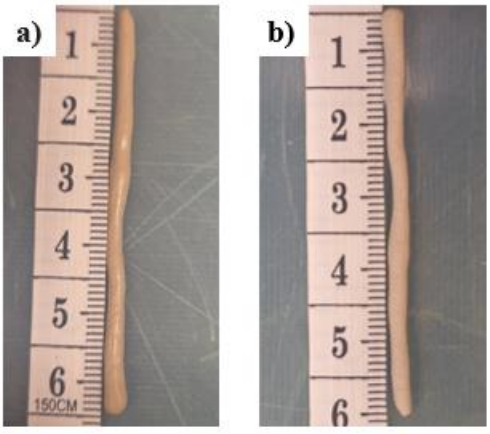

Figure 53a and b Pyrolysis of Ink D (a) before and (b) after pyrolysis at 1000 ℃, 1 ℃/min, and 1 hour dwell time.

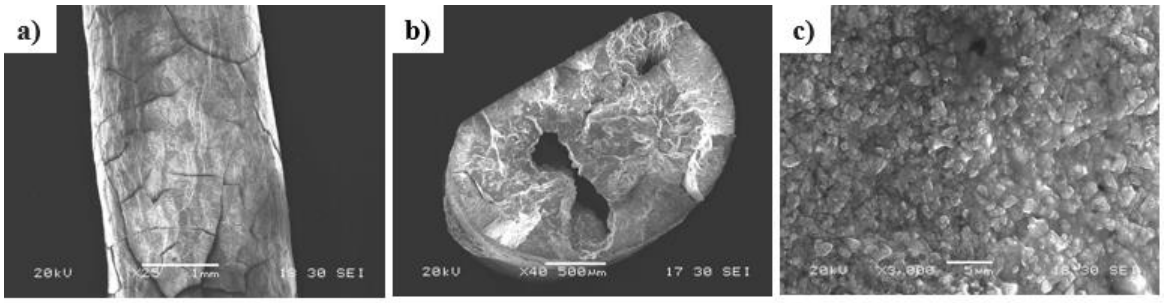

Figure 54a, b, and c SEM images of Ink D at 1000 ℃, 1 ℃/min, and 1 hour dwell time. (a) Surface image at 25x magnification and 1mm scale. (b) Broad cross-sectional image taken at 40x magnification and 500µm scale. (c) close-up cross-sectional image taken at 3000x magnification and 5µm scale.

Figure 55a and b show Ink E before and after pyrolysis respectively. Ink E failed under the pyrolysis conditions depicted in Table 12. Much like Ink B, Ink E failed in such a way that the sample had completely adhered to the furnace block the sample was placed on. This indicates that increasing the amount of MK solution present in the ink will increase the possibility of failure upon pyrolysis. The results from Ink F and other tests will help to confirm or deny this theory. While Ink E did fail it was possible to scrape off a small sample from the furnace block to perform SEM imaging. Continuing to observe the outward appearance of the samples, it is noticed that a color change took place before and after pyrolysis, a clear sign of a chemical change. This color change means that the preceramic polymer used in this study was successfully converted into a SiC ceramic. After analyzing the outward appearance of Ink E, the next step is analyzing the ink remains using the SEM machine. Figure 56a shows an image of the surface of Ink E, at 25x magnification and 1mm scale. From the broad view of the surface, it could be seen that the while the sample does have a smooth surface, there are too many cracks and pores to draw any more conclusions about the effect of SiC on a sample. Figure 56b shows a closer view

of a crack on the surface of Ink E, at 5000x magnification and 5µm scale. This granular surface seen on the inside of the crack is consistent with the surface quality at high magnifications as seen in Ink D.

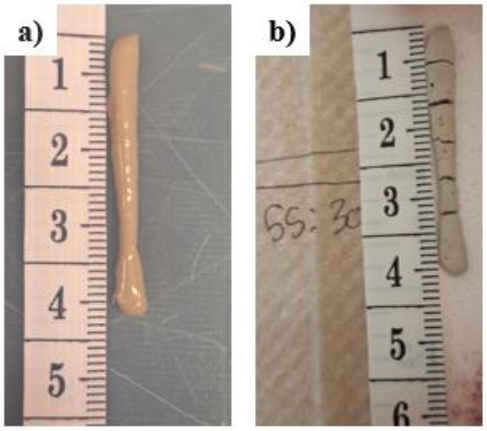

Figure 55a and b Pyrolysis of Ink E (a) before and (b) after pyrolysis at 1000 ℃, 1 ℃/min, and 1 hour dwell time.

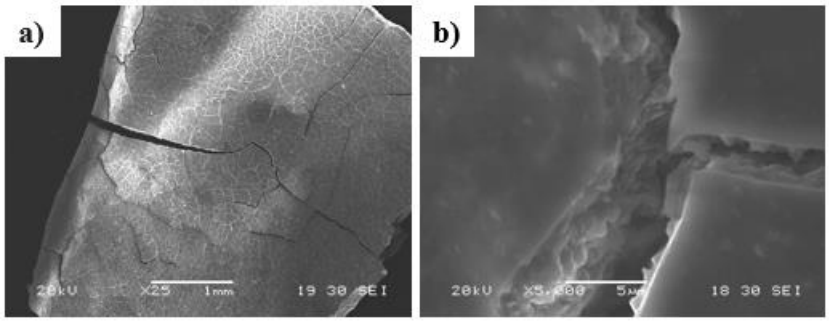

Figure 56a and b SEM images of Ink E at 1000 ℃, 1 ℃/min, and 1 hour dwell time. (a) Surface image at 25x magnification and 1mm scale. (b) close-up surface image taken at 5000x magnific1ation and 5µm scale.

Figure 57a and b show Ink F before and after pyrolysis respectively. Ink F failed under these pyrolysis conditions depicted in Table 9. Much like Ink B and E, Ink F failed in such a way that

the sample had completely adhered to the furnace block the sample was placed on. This indicates that by increasing the amount of MK solution present in the ink, it will have a greater possibility to fail upon pyrolysis. This further supports the results that as less SiC is added the more likely the sample is to fail. Unlike Inks B and F, no sample fragments were able to be retrieved to perform SEM imaging on. Continuing to observe the outward appearance of the samples, it is noticed that a color change took place before and after pyrolysis, just like all other inks, this is a clear sign of a chemical change. This color change means that the preceramic polymer used in this study was successfully converted into a SiC ceramic.

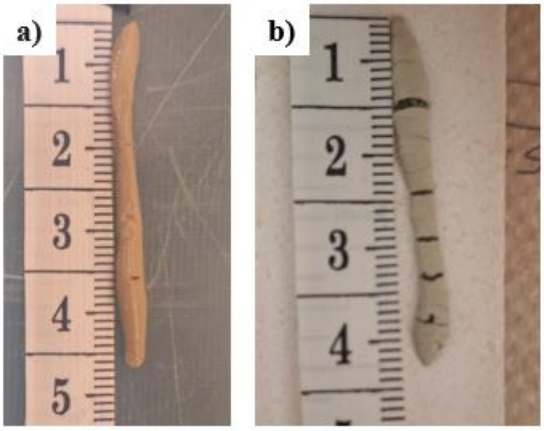

Figure 57a and b Pyrolysis of Ink F (a) before and (b) after pyrolysis at 1000 ℃, 1 ℃/min, and 1 hour dwell time.

3.3.3.3 Conclusion - Effect of SiC at Varying Max Temperature

From the pyrolysis results of Inks D, E, and F and tests 2 and 3 it can be concluded that as less SiC is added the final ceramic structure becomes increasingly unstable. Based on rheology Inks D and E both had shear thinning and no crossover region, while Ink F was shear thickening, and did contain a crossover point. This indicates that shear thinning is a larger contribution to

determining an inks success than crossover point. However, since Ink E had shear thinning this means that it should have succeeded during pyrolysis. Since Ink E failed it can be concluded that this was due to the lower amount of SiC present within the ink formula. This narrows down the ideal MK to SiC ratio to be closer to 45MK:55SiC as this ink's structure consistently held up at varying temperatures at this ratio.

3.3.4 Role of Fumed Silica Based on Inks G and H at 1300 ℃ and 1000 ℃

3.3.4.1 Test 2 Inks G and H at 1300 ℃

Inks G and H underwent the same parameters outlined in Table 8. The pyrolysis results for Inks G and H are illustrated in Figures 58 a and b, Figures 59 a and b for Ink G and Figures 60 a and b and Figure 61 a and b for Ink H. Ink G before and after pyrolysis, Figure 58a and b, underwent an overall linear shrinkage of 4.813 mm or 10.69%. which is consistent with the expected dimensional changes and the piece had also observed the color change needed to prove that a ceramic was formed. SEM machine analysis of the ink is in Figure 59a showing the surface at 50x magnification and 500µm scale. The two most notable features are a large crack and the agglomerates along the surface. These agglomerates were likely formed either because of improper mixing or because of an unknown chemical reaction. Figure 59b shows an image of the cross-section of Ink G, at 65x magnification and 200µm scale with the presence of smooth structure present indicating a fully formed ceramic. The surface structure/quality seen in Ink G was an improvement from the previous inks tested. And while the cracking of Ink G is more severe, the cracks are more uniform and tend to segment the sample better than the other samples. This controlled cracking is an indication that the ceramic formed in larger segments

before being broken by thermal cracks. Unlike the prior samples, there appear to be no pores indicating that fumed silica does improve the structure of the sample output. It is concluded that these results are an improvement in this ink formula, based off of (Ink D).

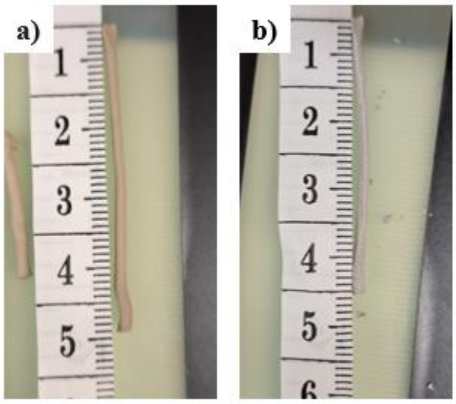

Figure 58a and b Pyrolysis of Ink G (a) before (b) after pyrolysis at 1300 ℃, 1 ℃/min, 1 hour

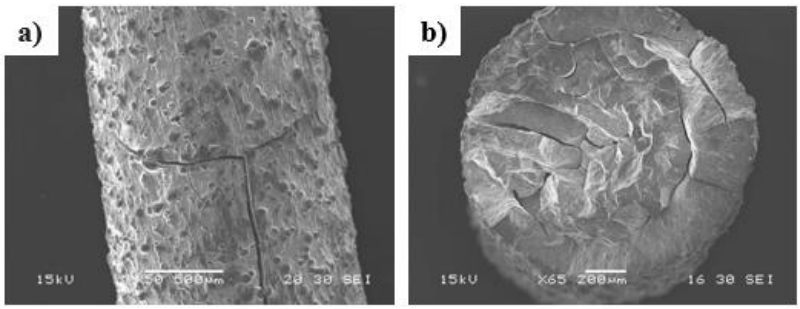

Figure 59a and b SEM images of Ink G at 1300 ℃, 1 ℃/min, and 1 hour dwell time. (a) Surface image at 50x magnification and 500µm scale. (b) Broad cross-sectional image taken at 65x magnification and 200µm scale.

Ink H's overall linear shrinkage was 5.541 mm or 12.49%. Figure 61a shows an image of the surface of Ink H, at 25x magnification and 1mm scale on the SEM microscope. The cracks are smaller but there are still agglomerates, although visibly fewer than those seen on Ink's G's surface. In looking at a close-up image, Figure 61 b, the crack can be seen on the surface of Ink

H, at 300x magnification and 50µm scale. An image of the cross-section was unable to be obtained due to the fragility of the sample. However, this ink formulation is still significant progress towards the creation of a usable ceramic slurry. While there are still some issues with Ink H it appears the addition of fumed silica allowed for the ceramic structure to stabilize more than if there was no fumed silica added.

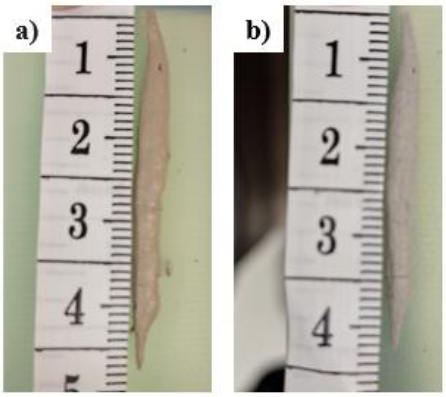

Figure 60a and b Pyrolysis of Ink H (a) before and (b) after pyrolysis at 1300 ℃, 1 ℃/min, and 1 hour dwell time.

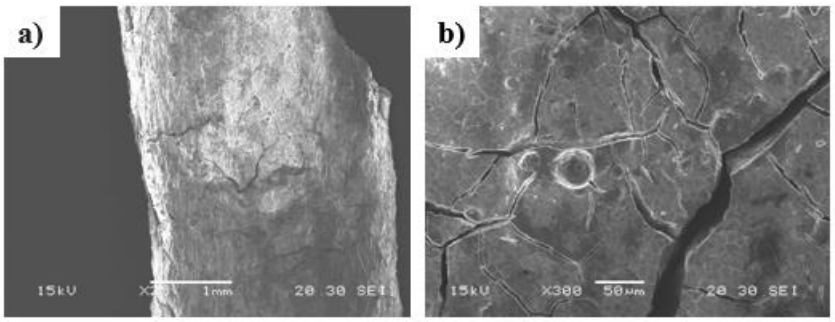

Figure 61a and b SEM images of Ink H at 1300 ℃, 1 ℃/min, and 1 hour dwell time. (a) Surface image at 25x magnification and 1mm scale. (b) Broad cross-sectional image taken at 300x magnification and 50µm scale.

3.3.4.2 Test 3 Inks G and H at 1000 ℃

Inks G and H underwent pyrolysis with the specific parameters outlined in Table 9. The pyrolysis results for Inks G and H are illustrated in Figures 62 a and b, Figures 63 a and b for Ink G and Figures 64 a and b and Figure 65 a and b for Ink H.

Figure 62a and b show Ink G before pyrolysis and after pyrolysis respectively, and by comparing these two images it can be observed that Ink G underwent an overall linear shrinkage of 2.712 mm or 6.96%. This level of shrinkage is consistent with the expected dimensional changes typically observed in SiC ceramic parts during pyrolysis. The controlled shrinkage observed in this sample suggests that the pyrolysis treatment was effective in maintaining the structural integrity of the ceramic while reducing its size within anticipated limits. It can also be observed that a color change took place before and after pyrolysis, this is a clear sign of a chemical change. It is important to note that a chemical change occurred because this leads to further proof that a ceramic was formed. This color change means that the preceramic polymer used in this study was successfully converted into a SiC ceramic. After analyzing the outward appearance of Ink G, the next step was analyzing the Ink using the SEM machine. Figure 63a shows an image of the surface of Ink G, at 30x magnification and 500µm scale. Looking at the surface the two most notable features are the large crack and the agglomerates along the surface. These agglomerates are likely formed because of improper mixing or form because of an unknown chemical reaction. Figure 63b shows an image of the cross-section of Ink G, at 60x magnification and 200µm scale. From the broad view of the cross-section the sample is seen to have a smooth structure present in the cross-section. This smooth structure, much like Ink A and B, means that the ceramic structure has fully formed at this temperature. While the surface

quality is not as good as that seen in test 2 due to the large pore, it is still one of the better cross-sections observed in this study. And while the cracking of Ink G is more severe, the cracks are more uniform and tend to segment the sample better than the other samples. This controlled cracking is an indication that the ceramic forms in larger segments before being broken by thermal cracks. Unlike other samples in this study there appear to be no pores in this sample. These observations indicate that fumed silica does improve the structure of the sample, as these results are an improvement from the Ink D formula, the one this ink is based off.

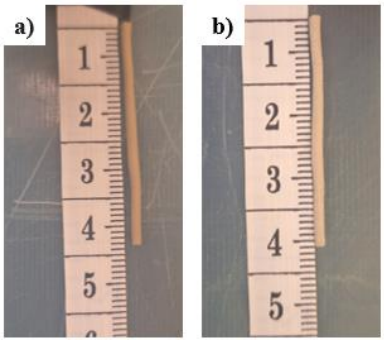

Figure 62a and b Pyrolysis of Ink G (a) before and (b) after pyrolysis at 1000 ℃, 1 ℃/min, and 1 hour dwell time.

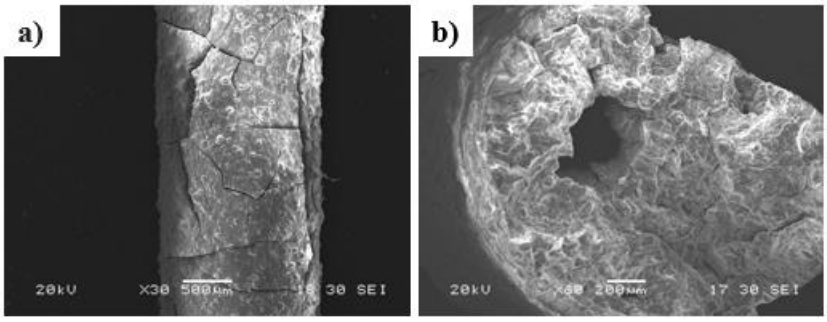

Figure 63a and b SEM images of Ink G at 1000 ℃, 1 ℃/min, and 1 hour dwell time. (a) Surface image at 30x magnification and 500µm scale. (b) Broad cross-sectional image taken at 60x magnification and 200µm scale.

Figure 64a and b pre and post pyrolysis show that Ink H underwent an overall linear shrinkage of 4.596 mm or 11.28%. This level of shrinkage is consistent with the expected dimensional changes typically observed in SiC ceramic parts during pyrolysis. The controlled shrinkage observed in this sample suggests that the pyrolysis treatment was effective in maintaining the structural integrity of the ceramic while reducing its size within anticipated limits. It was also observed that a color change took place before and after pyrolysis, a clear sign of a chemical change. It is important to note that a chemical change occurred because this leads to further proof that a ceramic was formed. This color change means that the preceramic polymer used in this study was successfully converted into a SiC ceramic. The ink sample when then analyzed using the SEM machine. Figure 65a shows an image of the surface of Ink H, at 30x magnification and 500µm scale. Looking at the surface the most notable feature are the large cracks along the surface of the part. However, unlike in test 2, Ink H does not contain any visible agglomerates on the surface of the part. Figure 65b shows a cross-sectional image of Ink H, at 33x magnification and 500µm scale. Unlike test 2, an image of the cross-section was able to be obtained. One of the best features of this cross-section is the smoothness. This indicates the ceramic formed fully in nearly one whole part with minimal cracking. The worst feature of the cross-section are the voids seen on the left side of the cross-sectional image. These voids are an indication that the sample is hollow to begin with. And therefore, the major reason Ink F keeps failing in the furnace is because it is hollow on the inside. However, Ink H was able to achieve partial success due to the fumed silica that is added. This is significant progress towards creating a usable ceramic slurry because the ink formula that Ink H is based on, Ink F, was unable to be viewed in the SEM machine after sample failure. While there are still some issues with Ink H it appears the addition of fumed silica allowed for the ceramic structure to stabilize more than if there was no fumed

silica added.

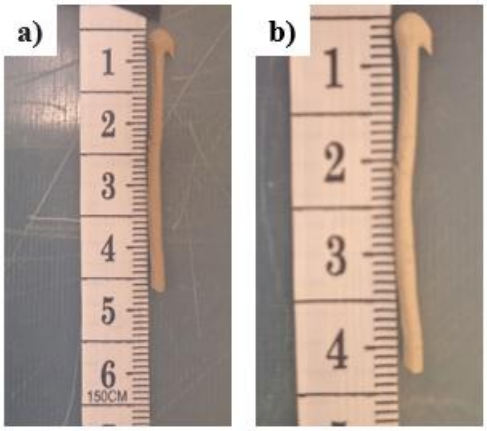

Figure 64a and b Pyrolysis of Ink H (a) before and (b) after pyrolysis at 1000 ℃, 1 ℃/min, and 1 hour dwell time.

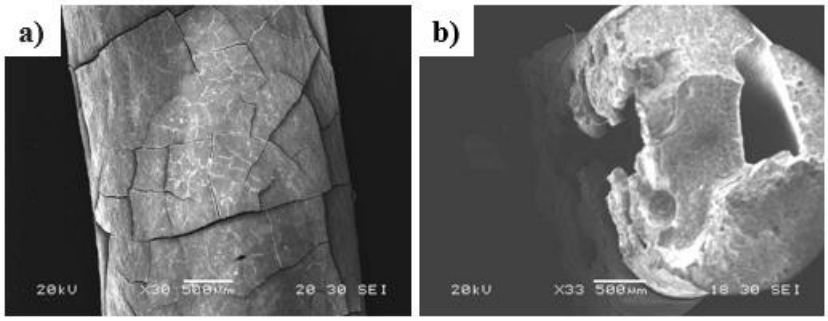

Figure 65a and b SEM images of Ink H at 1000 ℃, 1 ℃/min, and 1 hour dwell time. (a) Surface image at 30x magnification and 500µm scale. (b) Broad cross-sectional image taken at 33x magnification and 500µm scale.

3.3.4.3 Conclusion – Effect of Fumed Silica on Inks G and H at 1300 ℃ and 1000 ℃

The results from tests 1 and 2 of Inks G and H indicate that fumed silica helps improve the structure of the final ceramic. Much like Inks A and B in the previous study, if we compare Inks

F and H it is possible to see a very similar conclusion. Inks F's structure had failed completely during pyrolysis much like Ink B, however by adding fumed silica, Ink H, the sample's structure stabilized enough to get SEM images of the surface and occasionally the cross section, similar to Ink A. This indicates that the conclusions drawn about fumed silica from Inks A and B are valid. From comparing these SEM images to those with just MK and SiC it can be seen that FS has a definite positive impact on improve the ceramic's structure and cracking.

3.3.5 Role of Carbon Fiber on Inks I, J, and K at 1300 ℃ and 1000 ℃

3.3.5.1 Test 2 Inks I, J, and K at 1300 ℃

Inks I, J, and K results with the same testing parameters are shown in Figures 66 a and b, Figures 67 a, b, and c for Ink I, Figures 68 a and b and Figures 69 a and b for Ink J, and Figures 70 a and b and Figures 71 a, b, and c for Ink K. Ink I underwent an overall linear shrinkage of 5.634 mm or 12.62% which was within parameters and had a successful color change which is shown in Figure 66a. The SEM machine using 2000x magnification and 10µm scale is seen in Figure 67a showing cracks still present in the outcome. Figure 67b shows an image of the cross-section of Ink I, at 220x magnification and 100µm scale. this cross-section highlights the size and number of pores, smooth structure presence, and holes left by the oxidized carbon fibers showing similar results to prior inks tested. The cracking was again less severe than those samples with just fumed silica indicating that the carbon fiber does seem to help hold the structure together early on but still oxidizes fully by the end leaving cracks in the outcome. This can be seen in Figure 67c which shows a cross-section of Ink I at a higher magnification, at 400x magnification and 50µm scale. You can see the holes the size of the milled carbon fibers used and that unlike in the

previous test of Ink A and B, there are no strands/remnants of carbon fiber that are sticking out from the holes. This indicates the temperature was too high and all the carbon fibers had completely oxidized before the SiC matrix had been fully formed but are still aligned directionally.

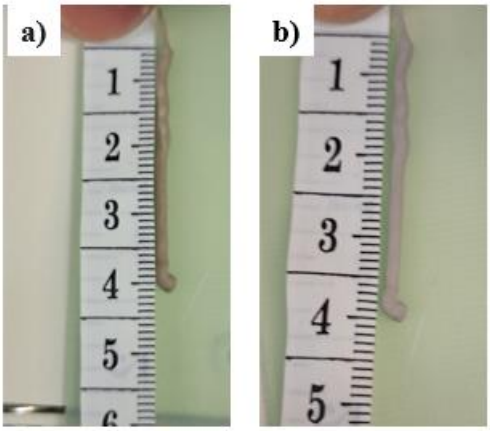

Figure 66a and b Pyrolysis of Ink I (a) before and (b) after pyrolysis at 1300 ℃, 1 ℃/min, and 1 hour dwell time.

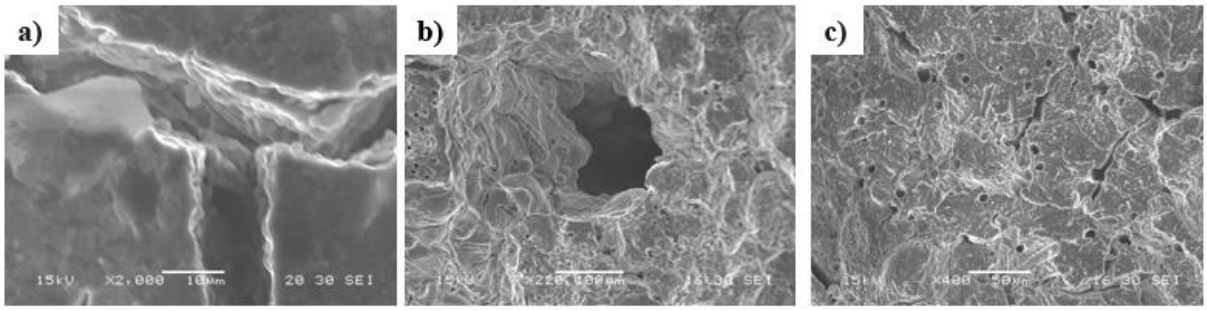

Figure 67a, b, and c SEM images of Ink I at 1300 ℃, 1 ℃/min, and 1 hour dwell time. (a) Surface crack image at 2000x magnification and 10μm scale. (b) Broad cross-sectional image taken at 220x magnification and 100μm scale. (c) close-up cross-sectional image taken at 400x magnification and 50μm scale.

Ink J as shown in Figure 68a and b underwent an overall linear shrinkage of 0.816 mm or 2.57% which is within acceptable parameters and completed the ceramic process conversion. There were fiber indents evident with most facing the direction of print. Because of this, there is a high probability the fibers are aligned in the cross-section as well. SEM analysis output at 250x magnification and 100µm scale is shown in Figure 69a with the same findings found including cracking, fiber indents, and no remnant fibers present. Figure 69b shows an image of the cross-section of Ink J, at 1000x magnification and 10µm scale. The cross section also showed similar outputs to the prior ink testing's including size and number of pores, the smooth structure presence, and holes left by the oxidized carbon fibers. Yet, while there are just as many pores present as in previous sample, the cracks are less severe than the sample with just fumed silica. Reinforcing prior findings that carbon fiber seems to help hold the structure together early in the pyrolysis process, but those fibers appear to oxidize fully before the matrix has fully formed when the temperature is too high. Another important observation while examining the cross-section is that many of the carbon fiber holes are all aligned in the same direction, the print direction. This is an important observation because it means that the shear stress created by the nozzle is sufficient to re-align the fibers in a uniform direction. Seeing the fibers align like this shows that Ink J has sufficient rheological properties to keep the fibers from re-orienting themselves once the Ink Leaves the nozzle.

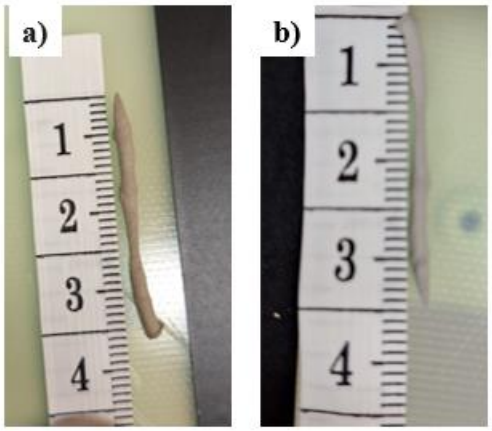

Figure 68a and b Pyrolysis of Ink J (a) before and (b) after pyrolysis at 1300 ℃, 1 ℃/min, and 1 hour dwell time.

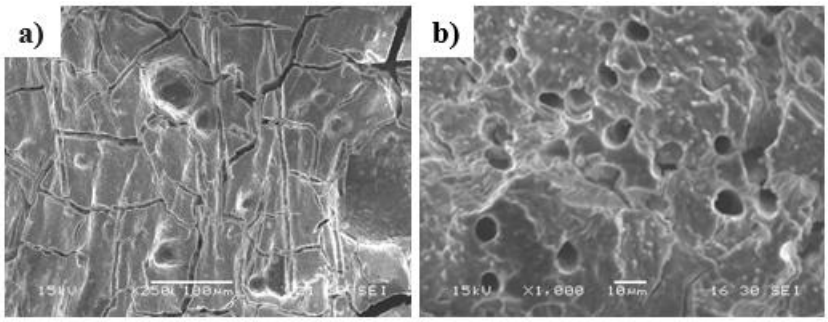

Figure 69a and b SEM images of Ink J at 1300 ℃, 1 ℃/min, and 1 hour dwell time. (a) Surface crack image at 250x magnification and 100µm scale. (b) close-up cross-sectional image taken at 1000x magnification and 10µm scale.

Figure 70a and b show Ink K before pyrolysis and after pyrolysis respectively and by comparing these two images it can be observed that Ink K underwent an overall linear shrinkage of 3.154 mm or 8.43%. This level of shrinkage is consistent with the expected dimensional changes typically observed in SiC ceramic parts during pyrolysis. The controlled shrinkage observed in this sample suggests that the pyrolysis treatment was effective in maintaining the structural

integrity of the ceramic while reducing its size within anticipated limits. It can also be observed that a color change took place before and after pyrolysis, a clear sign of a chemical change. It is important to note that a chemical change occurred because this leads to further proof that a ceramic was formed. This color change means that the preceramic polymer used in this study was successfully converted into a SiC ceramic as similar with the prior ink test outcomes. After analyzing the outward appearance of Ink K, the next step was to analyze the ink using the SEM machine. Figure 71a shows an image of the surface of Ink K, at 350x magnification and 50µm scale. From looking at the surface features, the most noticeable thing was the cracks that were present in the image and across the surface. This is a clear indication of some type of thermal stress or chemical imbalance within the ceramic matrix composites. Another noticeable surface feature is the indents where carbon fibers used to be present. Observing the fiber indents, most of them are going in the direction the sample was printed in, like the other inks that used carbon fiber. Figure 71b and c shows an image of the cross-section of Ink K, at two different magnifications. Pore size, crack presence, ceramic solid presence, and missing carbon remnants outcomes were similar to Ink I and J.

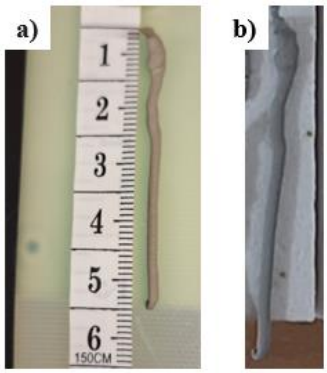

Figure 70a and b Pyrolysis of Ink K (a) before and (b) after pyrolysis at 1300 ℃, 1 ℃/min, and 1 hour dwell time.

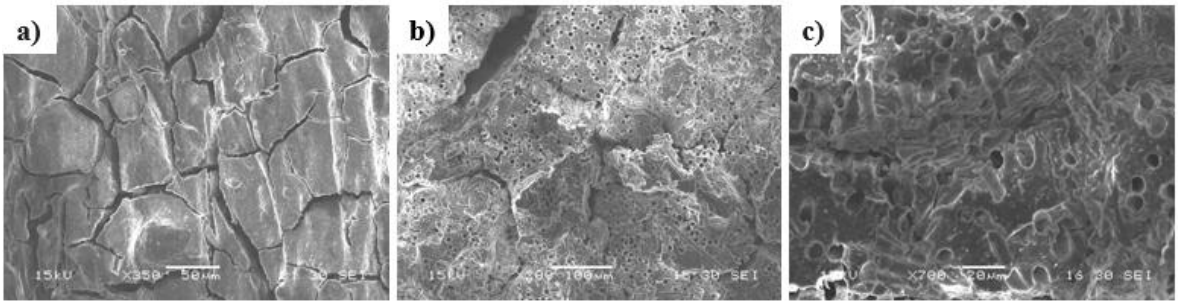

Figure 71a, b, and c SEM images of Ink K at 1300 ℃, 1 ℃/min, and 1 hour dwell time. (a) Surface image at 350x magnification and 50µm scale. (b) Broad cross-sectional image taken at 200x magnification and 100µm scale. (c) close-up cross-sectional image taken at 700x magnification and 20µm scale.

3.3.5.2 Test 3 Inks I, J, and K at 1000 ℃

Inks I, J, and K were the next samples to undergo pyrolysis with the specific parameters outlined in Table 9. The pyrolysis results for Inks I, J, and K are illustrated in Figures 72 a and b. Figures 73 a, b, and c represent Ink I and Figures 74 a and b and Figures 75 a, b, and c are results from for Ink J. Lastly, Figures 76 a and b and Figures 77 a, b, and c are for Ink K. Figure 72a and b show Ink I before and after pyrolysis with an overall linear shrinkage of 1.332 mm or 4.22%. This level of shrinkage is consistent with the expected dimensional changes and color changing are consistent with ceramic pyrolysis testing outcomes. Figure 73a shows a broad surface image of Ink I using the SEM at a 30x magnification and 200µm scale. Like other samples, the outcomes seen were cracks that are present across the surface, giving a clear indication of some type of thermal stress or chemical imbalance within the ceramic matrix composites. Figure 73b shows an image of the cross-section of Ink I, at 70x magnification and 200µm scale with similar testing outcomes. From the cross-section there were three things that stand out, the size and

number of the pores, the smooth structure present in the cross-section, and the holes left by the oxidized carbon fibers. This sample has a smooth cross-section surface structure meaning that the ceramic structure was fully formed. There are just as many pores present as in previous sample, however the cracks are less severe than those samples with just fumed silica. Reinforcing the outcome that carbon fiber seems to help hold the structure together and cause fewer large cracks even within different testing parameters. However, the fibers seem to help only early on because by the end of the pyrolysis process the fibers appear to oxidize fully. The oxidized fibers leave behind holes the exact size of the fibers, just like Inks A and B. Figure 73c at a higher magnification of 400x magnification and 50μm scale show small holes that seem to be everywhere in the cross-section with no strands/remnants of carbon fiber sticking out. This indicates that the temperature was too high and so all the carbon fibers had completely oxidized before the SiC matrix had been fully formed. Another important observation while examining the cross-section is that many of the carbon fiber holes are all aligned in the same direction, the print direction. This is an important observation because it means that the shear stress created by the nozzle is sufficient to re-align the fibers in a uniform direction. Seeing the fibers align like this also shows that Ink I has sufficient rheological properties to keep the fibers from re-orienting themselves once the Ink Leaves the nozzle.

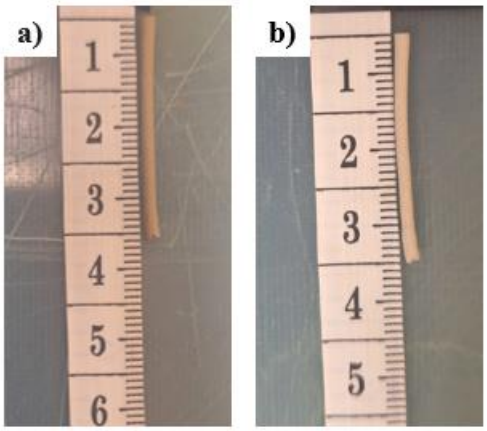

Figure 72 a and b Pyrolysis of Ink I (a) before and (b) after pyrolysis at 1000 ℃, 1 ℃/min, and 1 hour dwell time.

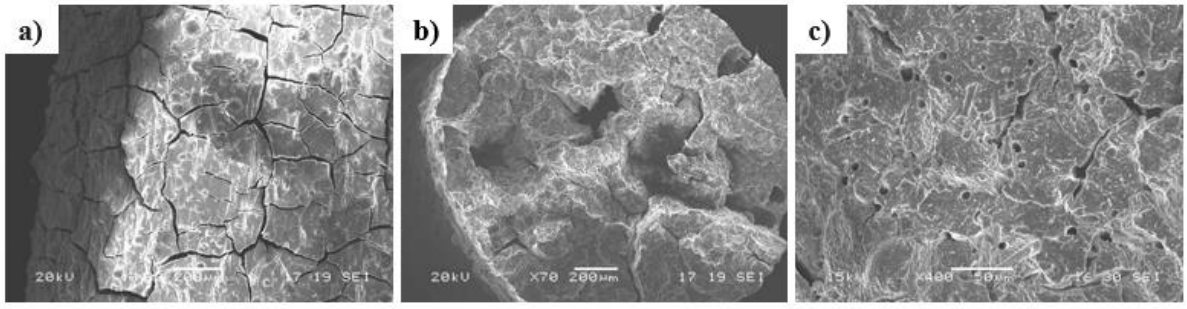

Figure 73a, b, and c SEM images of Ink I at 1000 ℃, 1 ℃/min, and 1 hour dwell time. (a) Surface image at 30x magnification and 200µm scale. (b) Broad cross-sectional image taken at 70x magnification and 200µm scale. (c) close-up cross-sectional image taken at 400x magnification and 50µm scale.

Figure 74a and b show Ink J before and after pyrolysis showing that Ink J underwent an overall linear shrinkage of 3.765 mm or 9.69%. This level of shrinkage is consistent with the expected dimensional changes typically observed in SiC ceramic parts during pyrolysis. The controlled shrinkage observed in this sample suggests that the pyrolysis treatment was effective in

maintaining the structural integrity of the ceramic while reducing its size within anticipated limits. It can also be observed that a color change took place before and after pyrolysis, this is a clear sign of a chemical change. It is important to note that a chemical change occurred because this leads to further proof that a ceramic was formed. This color change means that the preceramic polymer used in this study was successfully converted into a SiC ceramic. After analyzing the outward appearance of Ink J, the next step was to analyze the Ink using the SEM machine. Figure 75a shows that image of the surface of Ink J at 50x magnification and 500µm scale. Looking at the surface feature the most noticeable outcome is the presence of cracks, a clear indication of some type of thermal stress or chemical imbalance within the ceramic matrix composites. Figure 75b shows an image of the cross-section of Ink J, at 75x magnification and 200µm scale. The same three defining outcomes stood out as in prior tests. They were the size and number of the pores, the smooth structure present in the cross-section, and the holes left by the carbonized carbon fibers. There are also, as with prior tests, still some strands/remnants of carbon fiber that are sticking out from the holes with the remnants running in the same direction as seen in Figure 75c which shows an image of the surface of Ink J, at 700x magnification and 20µm scale.

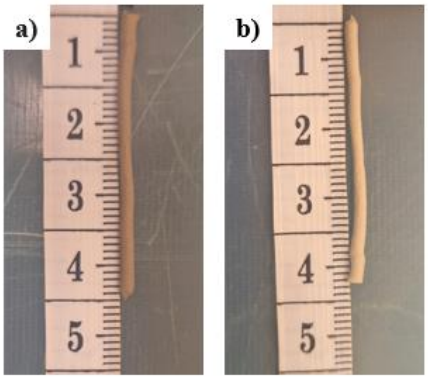

Figure 74a and b Pyrolysis of Ink J (a) before and (b) after pyrolysis at 1000 ℃, 1 ℃/min, and 1 hour dwell time.

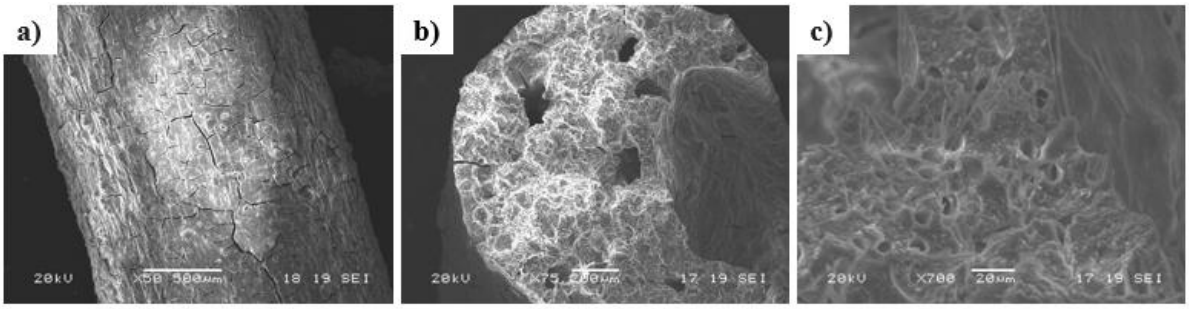

Figure 75a, b, and c SEM images of Ink J at 1000 ℃, 1 ℃/min, and 1 hour dwell time. (a) Surface image at 50x magnification and 500µm scale. (b) Broad cross-sectional image taken at 75x magnification and 200µm scale. (c) close-up cross-sectional image taken at 700x magnification and 20µm scale.

Figures 76a and b show Ink K before and after pyrolysis observing that Ink K underwent an overall linear shrinkage of 3.643 mm or 10.03%. This level of shrinkage is consistent with the expected dimensional changes typically observed in SiC ceramic parts during pyrolysis. The controlled shrinkage observed in this sample suggests that the pyrolysis treatment was effective in maintaining the structural integrity of the ceramic while reducing its size within anticipated

limits. It can also be observed that a color change took place before and after pyrolysis, this is a clear sign of a chemical change. It is important to note that a chemical change occurred because this leads to further proof that a ceramic was formed. This color change means that the preceramic polymer used in this study was successfully converted into a SiC ceramic. After analyzing the outward appearance of Ink K, the ink was analyzed using the SEM machine. Figure 77a shows an image of the surface of Ink K at 130x magnification and 100µm scale. From looking at the surface features one of the most noticeable things is that cracks that are present across the surface, a clear indication of some type of thermal stress or chemical imbalance within the ceramic matrix composites. Another noticeable surface feature is the indents where carbon fibers used to be present. Observing the fiber indents, most of them are going in the direction the sample was printed in, much like the other inks that used carbon fiber. Since these fibers are aligned in the print direction on the surface, there is a high probability they are aligned in the cross-section as well. Figure 77b shows an image of the cross-section of Ink K, at 85x magnification and 200µm scale. From the cross-section there were three things that stood out and they were the size and number of the pores, the smooth structure present in the cross-section, and the holes left by the carbonized carbon fibers. This sample has a smooth cross-section surface structure meaning that the ceramic structure was fully formed. There are just as many pores present as in previous sample, however the cracks are less severe than the samples with fumed silica. This indicates that carbon fiber seems to help hold the structure together and cause fewer large cracks. However, the fibers seem to help early on because by the end of the pyrolysis process the fibers appear to oxidize fully. The oxidized fibers leave behind holes the exact size of the fibers, just like Inks A and B. Figure 77c shows an image of the cross-section of Ink A at a higher magnification, at 350x magnification and 50µm scale. In this last image it is

important to note the small holes that seem to be everywhere in the cross-section were found to be the exact size of the milled carbon fibers used in the ink. And much like Ink I, there was no strands/remnants of carbon fiber that are sticking out from the holes. This is an indication that the temperature was too high, and all the carbon fibers had completely oxidized before the SiC matrix had been fully formed. The holes aligning in the same direction, the print direction, also means that the shear stress created by the nozzle is sufficient to re-align the fibers in a uniform direction. Seeing the fibers align like this also shows that Ink K has sufficient rheological properties to keep the fibers from re-orienting themselves once the Ink Leaves the nozzle.

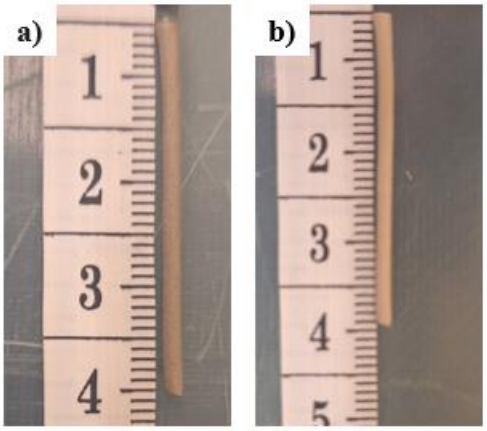

Figure 76a and b Pyrolysis of Ink K (a) before and (b) after pyrolysis at 1000 ℃, 1 ℃/min, and 1 hour dwell time.

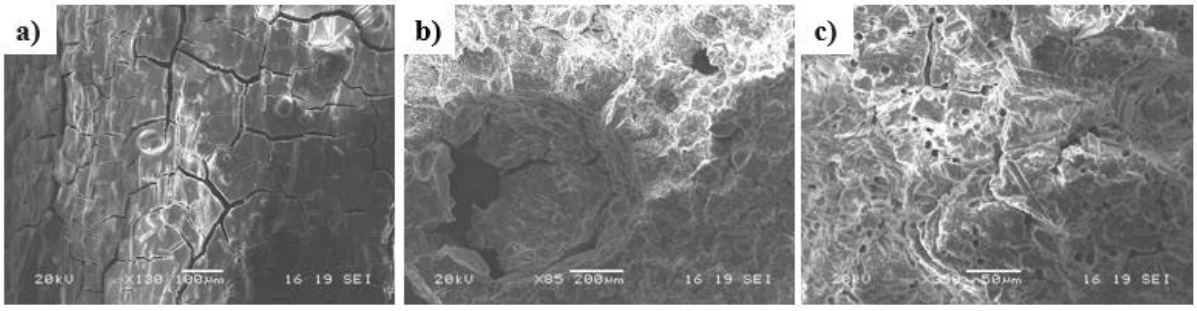

Figure 77a, b, and c SEM images of Ink K at 1000 ℃, 1 ℃/min, and 1 hour dwell time. (a) Surface image at 130x magnification and 100µm scale. (b) Broad cross-sectional image taken at 85x magnification and 200µm scale. (c) close-up cross-sectional image taken at 350x magnification and 50µm scale.

3.3.5.3 Conclusion – Effect of Carbon Fiber on Inks I, J, and K at 1300 ℃ and 1000 ℃

Based on the results of Inks I, J, and K at varying temperatures, carbon fiber has a positive impact on the overall structure of the final ceramic no matter the temperature. The cross-section of each ink experiences less cracking as more carbon fiber is added. However, the problem of the carbon fibers oxidizing still remains, as seen in the results from Inks A and B. This indicates that the loss of fibers is not due to any discrepancies in Ink formulation or temperature. This is why the next set of tests will focus on changing the ramp rate of pyrolysis. Ink K will be used for these tests as it is the ink formula that contains the most carbon fibers.

3.3.6 Ramp Rates Impact on Fiber Loss

3.3.6.1 Role of Ramp Rate on Ink K at 10 ℃/min

The next pyrolysis test of Ink K was conducted under the specific parameters outlined in Table

10. These conditions were determined by going to the minimum temperature pyrolysis could be achieved at according to other studies and modifying the rate the test was conducted at. The ramp rate was increased to 10 ℃/min as it was theorized that by increasing the rate it became possible for the ceramic to form/cure faster and protect the fibers from oxidizing.

Figure 78a and b show Ink K before and after pyrolysis showing that Ink K underwent an overall linear shrinkage of 1.97 mm or 3.48%. This level of shrinkage is consistent with the expected dimensional changes typically observed in SiC ceramic parts during pyrolysis. The controlled shrinkage observed in this sample suggests that the pyrolysis treatment was effective in maintaining the structural integrity of the ceramic while reducing its size within anticipated limits. It can also be observed that a color change took place before and after pyrolysis, this is a clear sign of a chemical change. It is important to note that a chemical change occurred because this leads to further proof that a ceramic was formed. This color change means that the preceramic polymer used in this study was successfully converted into a SiC ceramic. After analyzing the outward appearance of Ink K, the ink was looked at using the SEM machine. Figure 79a shows a broad surface image of Ink K, at 50x magnification and 500µm scale. From looking at the surface feature the most noticeable thing is the cracks that are present in the image. These cracks are less severe than those seen in other samples indicating that the new carbon fiber is either helping the structure, or the effect could be due to the low processing temperature. Also visible from examining the surface is the remnants of oxidized carbon fibers, as seen in the yellow circles in Figure 80. This is evidence that some fibers have survived these pyrolysis conditions. Figure 79b shows an image of the cross-section of Ink K at 85x magnification and 200µm scale. From the cross-section there were three things that stood out; the size and number

of the pores, the smooth structure present in the cross-section, and the holes left by the oxidized carbon fibers. This sample has a smooth cross-section surface structure meaning that the ceramic structure was fully formed. The pores seen in the sample are far smaller and less numerous than those seen in other samples. This could be a result of the new carbon fiber, or it may have been the new mixing protocol. Another observation was that there were significantly less cracks on the cross-section of the surface, compared to inks without fiber. This indicates that carbon fiber seems to help hold the structure together and cause fewer large cracks. However, the fibers seem to help early on because by the end of the pyrolysis process some fibers appear partially oxidized. The partially oxidized fibers leave behind holes the exact size of the fibers, and unlike most inks in this study small strands could be seen indicating that the fibers had not fully oxidized. Figure 79c shows an image of the cross-section of Ink K at a higher magnification, at 300x magnification and 50μm scale. In this last image it is important to note the small holes that seem to be everywhere in the cross-section. These holes, upon measuring them, were found to be the exact size of the milled carbon fibers used in the ink. Unlike the previous test some of the holes contained very small strands of fiber, however upon zooming in on these strands they were no longer visible. The cause of this phenomenon is unknown. Another important observation while examining the cross-section is that many of the carbon fiber holes are all aligned in the same direction, the print direction. This is an important observation because it means that the shear stress created by the nozzle is sufficient to re-align the fibers in a uniform direction. Seeing the fibers align like this also shows that Ink K has sufficient rheological properties to keep the fibers from re-orienting themselves once the Ink K leaves the nozzle.

These results indicate that lowering the carbon content of the fiber did not help to prevent the

carbon fibers from oxidizing or it could be that the carbon content was not low enough to have a significant impact. And it is further believed from these results that increasing the rate of the test only marginally helps protect the fibers from oxidizing.

Table 10 Pyrolysis Parameters for Test 4

Ink	Max Temperature (℃)	Ramp Rate (℃/min)	Dwell Time (Hour)	Environment
K	800	10	1	Air

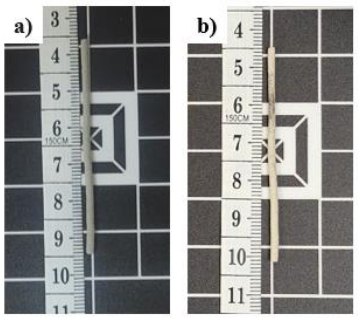

Figure 78a and b Pyrolysis of Ink K (a) before (b) after pyrolysis at 800 ℃, 10 ℃/min, 1 hour

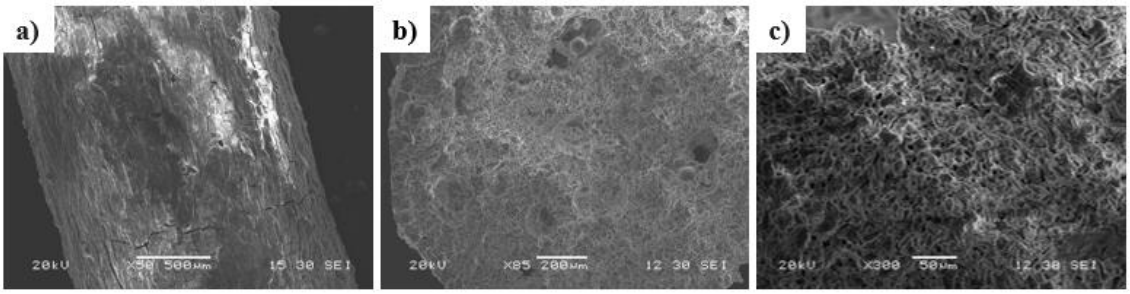

Figure 79a, b, and c SEM images of Ink K at 800 ℃, 10 ℃/min, and 1 hour dwell time. (a) Surface image at 50x magnification and 500µm scale. (b) Broad cross-sectional image taken at 85x magnification and 200µm scale. (c) close-up cross-sectional image taken at 300x magnification and 50µm scale.

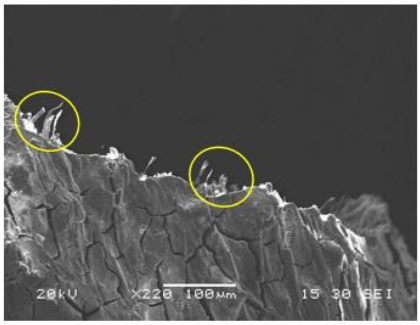

Figure 80 SEM images of Ink K at 800 ℃, 10 ℃/min, and 1 hour dwell time taken at 220x magnification and 100µm scale. Yellow circles highlight the partially oxidized carbon fibers.

3.3.6.2 Role of Ramp Rate on Ink K at 20 ℃/min

The next pyrolysis test of Ink K was conducted under the specific parameters outlined in Table 11. These conditions were determined by going to the minimum temperature pyrolysis could be achieved at according to other studies and modifying the rate this test was conducted at. The ramp rate was increased to 20 ℃/min as it was theorized that by increasing the rate even more it is possible for the ceramic to form/cure faster and protect the fibers from oxidizing.

Figure 81a and b show Ink K before and after pyrolysis showing Ink K underwent an overall linear shrinkage of 1.756 mm or 5.24%. This level of shrinkage is consistent with the expected dimensional changes typically observed in SiC ceramic parts during pyrolysis. The controlled shrinkage observed in this sample suggests that the pyrolysis treatment was effective in maintaining the structural integrity of the ceramic while reducing its size within anticipated limits. It can also be observed that a color change took place before and after pyrolysis, this is a clear sign of a chemical change. It is important to note that a chemical change occurred because this leads to further proof that a ceramic was formed. This color change means that the

preceramic polymer used in this study was successfully converted into a SiC ceramic. In Figure 81b it is possible to see a crack in the sample. This was not formed because of pyrolysis. The sample broke due to improper handling. After analyzing the outward appearance of Ink K, the next step was analyzing the Ink using the SEM machine. Figure 82a shows a broad surface image of Ink K at 120x magnification and 100µm scale. From looking at the surface feature the most noticeable thing is the cracks that are present in the image. These cracks are more severe than those seen on the surface of Ink K in test 4. This seems to indicate that increasing the rate will most likely not help in preventing the carbon fibers from oxidizing. Figure 82b shows an image of the cross-section of Ink K, at 70x magnification and 200µm scale. From the cross-section there were three things that stood out and they were the size and number of the pores, the smooth structure present in the cross-section, and the holes left by the oxidized carbon fibers. This sample has a smooth cross-section surface structure meaning that the ceramic structure was fully formed. The pores seen in the sample are far smaller and less numerous than those seen in other samples. This could be a result of the new carbon fiber or that the sample was mixed better than the others. Another observation is that there are significantly less cracks on the cross-section of the surface, compared to inks without fiber. This indicates that carbon fiber seems to help hold the structure together and cause fewer large cracks. However, the fibers seem to only assist early on because by the end of the pyrolysis process some fibers appear fully oxidized. The fully oxidized fibers leave behind holes the exact size of the fibers used in the ink formula. Figure 82c shows an image of the cross-section of Ink K at a higher magnification, at 250x magnification and 100µm scale. In this image it is important to note the small holes that seem to be everywhere in the cross-section. These holes, upon measuring them, were found to be the exact size of the milled carbon fibers used in the ink. Unlike the previous test no strands of oxidized fiber were

found by examining the edge of the surface or the cross-section. Another important observation while examining the cross-section is that many of the carbon fiber holes are all aligned in the same direction, the print direction. This is an important observation because it means that the shear stress created by the nozzle is sufficient to re-align the fibers in a uniform direction. Seeing the fibers align like this also shows that Ink K has sufficient rheological properties to keep the fibers from re-orienting themselves once the Ink Leaves the nozzle. These results indicate that increasing the rate too much will have a negative impact on the sample. This is an indication that optimizing the rate is not going to help prevent the fibers from oxidizing.

Table 11 Pyrolysis Parameters for Test 5

Ink	Max Temperature (℃)	Ramp Rate (℃/min)	Dwell Time (Hour)	Environment
K	800	20	1	Air

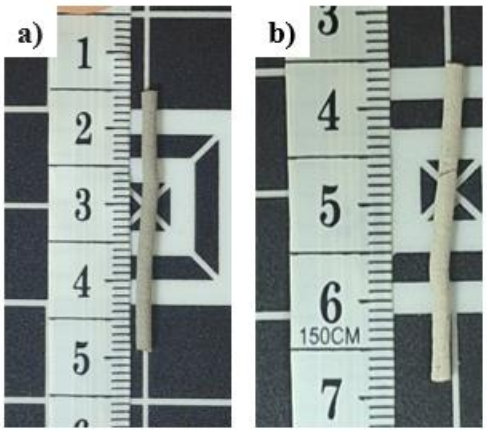

Figure 81a and b Pyrolysis of Ink K (a) before and (b) after pyrolysis at 800 ℃, 20 ℃/min, and 1 hour dwell time.

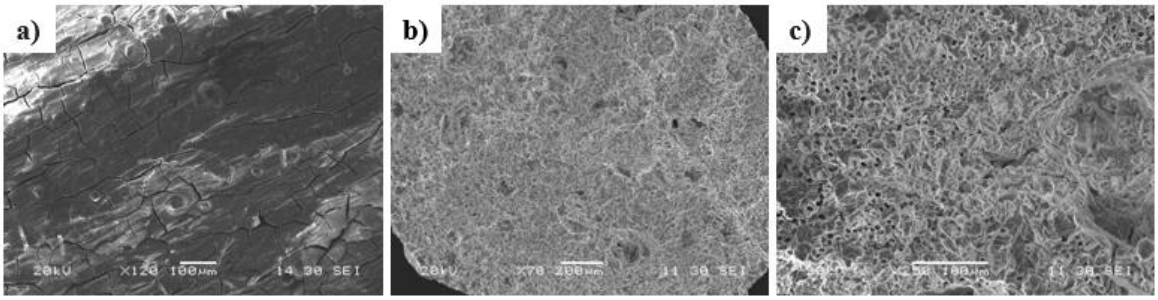

Figure 82a, b, and c SEM images of Ink K at 800 ℃, 20 ℃/min, and 1 hour dwell time. (a) Surface image at 120x magnification and 100µm scale. (b) Broad cross-sectional image taken at 70x magnification and 200µm scale. (c) close-up cross-sectional image taken at 250x magnification and 100µm scale.

3.3.6.3 Conclusions of the Ramp Rates Impact on the Final Ceramic

From the results from tests 4 and 5 it is possible to see that changing the ramp rate does not impact the visibility of the carbon fibers within Ink K. This indicates that the most likely reason that the fibers are oxidizing is due to the air environment that they are being pyrolyzed in.

CHAPTER 4: CONCLUSIONS AND FUTURE WORK

4.1 Rheological Property Conclusion

In the rheological testing of the slurries, a systematic approach was taken to assess the influence of various components on shear thinning and viscoelastic behavior. In the first step, the focus was on understanding the role of SiC in the slurry. Findings demonstrated that increasing the proportion of SiC in the mixture significantly enhanced shear thinning behavior, with the ideal ratio identified between 45MK:55SiC and 55MK:45SiC. The second phase of testing concentrated on the impact of FS, which proved effective in both improving shear thinning and providing favorable viscoelastic properties to the paste. Lastly, the contribution of C_f was evaluated. Although C_f did not produce any notable effect on the rheological behavior, its role was determined to be essential for achieving desirable final properties in the composite material.

4.2 Printing Conclusion

To prepare the samples for printing, it was determined that the initial step involved thoroughly mixing MK powder with IPA at a high rotational speed to form a uniform MK solution. This high-speed mixing was essential to ensure the consistency and homogeneity of the MK-IPA solution, which would directly impact the quality of the subsequent printed samples. Additionally, to streamline the early stages of pyrolysis testing, a custom syringe extruder was designed and constructed. This DIY extruder played a pivotal role in accelerating the pyrolysis process by enabling precise and controlled extrusion of the solution, facilitating more rapid testing cycles and allowing adjustments to be made as needed based on early results. By combining efficient solution preparation with this bespoke extrusion system, the overall workflow was optimized to support the demanding requirements of high-temperature testing and

material consistency.

4.3 Pyrolysis Conclusion

The study's findings on pyrolysis parameters offer insights into optimizing the structural integrity and stability of ceramic components within various ink formulations. Fumed silica was consistently shown to enhance ceramic structure by more closely binding its matrix, though it may require higher processing temperatures for complete ceramic formation. This led to a subsequent test conducted at an increased temperature and slower ramp rate to allow the ceramic matrix to develop fully. However, Ink B consistently failed across tests 2 and 3, suggesting it is not ideal for direct ink writing (DIW) applications. Rheology results further supported this conclusion, as Ink B demonstrated shear thickening behavior, making it less suited for stable flow under DIW. Despite containing a rheological crossover point—an indicator of potential structural stability—Ink B's flow behavior was shown to be a more critical factor, underscoring the importance of analyzing shear properties over crossover points.

A significant observation was the lack of visible carbon fibers across all inks and tests, likely due to oxidation during pyrolysis. This suggests that carbon fiber reinforcement might require adjustments to the pyrolysis environment to prevent oxidation. In analyzing the role of silicon carbide (SiC), Inks D, E, and F revealed that reducing SiC content led to a less stable final ceramic structure. Rheological testing showed that Inks D and E exhibited shear thinning and lacked a crossover region, while Ink F displayed shear thickening with a crossover point. These results imply that shear-thinning behavior contributes more significantly to an ink's success during DIW than the presence of a crossover point. Despite its shear-thinning behavior, Ink E failed, likely due to its lower SiC content, suggesting an optimal MK-to-SiC ratio of

approximately 45:55. This specific ratio was consistently stable across various temperature tests.

Fumed silica's benefits were further validated through comparisons between Inks G and H, and earlier Inks A and B. Ink F, lacking fumed silica, failed during pyrolysis similarly to Ink B, whereas the addition of fumed silica in Ink H stabilized the structure sufficiently to capture SEM images of both the surface and cross-section. This reinforces the conclusion that fumed silica significantly improves the ceramic structure, minimizing cracking and contributing to overall stability. Moreover, the study highlighted carbon fiber's positive impact on reducing cracking across the cross-section of ceramic structures, regardless of processing temperature, as observed in Inks I, J, and K. However, carbon fibers continued to oxidize, independent of ink formulation or temperature. Subsequent tests focused on varying the pyrolysis ramp rate for Ink K, which had the highest carbon fiber content, but changes in ramp rate did not affect carbon fiber visibility. This indicates that the oxidation of fibers is likely due to the pyrolysis environment, specifically the presence of air. These findings suggest that future tests should explore inert or reducing environments to prevent carbon fiber oxidation and further enhance ceramic integrity.

4.4 Future Directions

This study's findings offer contributions to material development that needs high toughness at elevated temperature, such as aerospace and nuclear industries. The insights into rheology, particularly the role of fumed silica (FS), demonstrate how specific additives can be used to achieve desired rheology properties. The study's emphasis on optimal SiC-to-matrix ratios and its exploration of ink formulations provide valuable data for creating ceramic structures with enhanced stability and crack resistance. Furthermore, the impact of pyrolysis conditions, particularly the environment on carbon fiber oxidation, presents practical guidance for engineers

seeking to use carbon fiber reinforcement without compromising structural integrity. By showing that careful ink formulation can improve rheological properties, the study provides a pathway to design durable, customizable ceramics suitable for precise additive manufacturing techniques. In high-temperature engineering, the recommendation to use inert atmospheres in pyrolysis could pave the way for more resilient, crack-resistant ceramics. These conclusions help to optimize the processing and composition of ceramic-based materials, contributing to advancements in the production of high-performance engineering materials.

Based on the preliminary result, the main objective will be to further mitigate cracking by investigating the origin of thermal stress. Future tasks will focus on the effects of the pyrolysis peak temperature, heating rate, and environments (e.g., Ar protective gas). Based on these results it is therefore hypothesized that the reason that severe carbon oxidization was seen may due to the type of environment used. The air environment is more likely to oxidize carbon than an inert environment (Nitrogen, Argon, etc.) would [36, 37, 53-56]. This is why future tests should be conducted in an inert environment to pyrolyze the samples, as these environments seem to limit the oxidation of carbon fibers.

The main objective is to investigate the role of carbon fiber dimensions and distribution in improving toughness in high-temperature applications. The toughness of these intrinsic strong materials could be significantly improved if carbon fibers were aligned and uniformly distributed with an optimized combination of dimension and density. The bonding between fiber and matrix, as well as the load transfer in composites will be investigated as well.

REFERNCES

1. Munz, D., *Failure criteria in ceramic materials.* Journal of Nuclear Materials, 1988. **155**: p. 77-81.
2. Li, L., *A micromechanical loading/unloading constitutive model of fiber-reinforced ceramic-matrix composites considering matrix crack closure.* Fatigue & Fracture of Engineering Materials & Structures, 2021. **44**(9): p. 2389-2411.
3. Raether, F., *CERAMIC MATRIX COMPOSITES- AN ALTERNATIVE FOR CHALLENGING CONSTRUCTION TASKS.* Ceramic Applications, 2013. **1**(1): p. 45-49.
4. Cambridge, *CES Selector*. 2009, Cambridge.
5. Ashby, M.F., *Materials selection in mechanical design.* Metallurgia Italiana, 1994. **86**: p. 475-475.
6. Naslain, R., *Ceramic matrix composites: matrices and processing.* Encyclopedia of Materials: Science and Technology, 2001: p. 1060-1066.
7. Lamon, J., *Reinforcement of ceramic matrix composites by ceramic continuous fibers*, in *Composite Reinforcements for Optimum Performance*. 2021, Elsevier. p. 55-93.
8. Zhang, L. and L. Cheng, *Discussion on strategies of sustainable development of continuous fiber reinforced ceramic matrix composites.* Acta Materiae Compositae Sinica, 2007. **24**(2): p. 1-6.
9. Swain, J., et al., *A brief review on ceramic matrix composites, it's attributes and it's utility in future generation gas turbine.* Inter J Innov Res in Sci Technol, 2014. **1**: p. 290-292.
10. Clauß, B., *Fibers for ceramic matrix composites*. 2008: Weinheim, Germany: WILEY-VCH Verlag GmbH & Co. KGaA.
11. Su, J., et al., *Al2O3 fiber-reinforced MAX phase ceramic matrix composite.* Ceramics International, 2024.
12. He, X.-b., et al., *Review of continuous fiber-reinforced ceramic matrix composites.* Cailiao Kexue yu Gongcheng(Materials Science and Engineering)(China)(China), 2002. **20**: p. 273-278.
13. Eswara Prasad, N., A. Kumar, and J. Subramanyam, *Ceramic matrix composites (CMCs) for aerospace applications.* Aerospace Materials and Material Technologies: Volume 1: Aerospace Materials, 2017: p. 371-389.
14. Kiratli, S., *An overview of the mechanical characterizations and applications of chopped fiber reinforced composites.* International Journal of Advanced Natural Sciences and Engineering Researches, 2023. **7**(4): p. 186-190.
15. Pienti, L., et al., *Effect of milling on the mechanical properties of chopped SiC fiber-reinforced ZrB2.* Materials, 2013. **6**(5): p. 1980-1993.
16. Kopeliovich, D., *Advances in the manufacture of ceramic matrix composites using infiltration techniques*, in *Advances in ceramic matrix composites*. 2014, Elsevier. p. 79-108.
17. Asmi, D. and I.M. Low, *Manufacture of graded ceramic matrix composites using infiltration techniques*, in *Advances in ceramic matrix composites*. 2014, Elsevier. p. 109-140.
18. Rayat, M.S., et al., *Fabrication and machining of ceramic composites—A review on current scenario.* Materials and Manufacturing Processes, 2017. **32**(13): p. 1451-1474.

19. Gupta, S., et al., *A Review of Additive Manufacturing Processes for Fabricating Ceramics and Composites.* AM&P Technical Articles, 2023. **181**(3): p. 23-27.
20. Franchin, G., L. Wahl, and P. Colombo, *Direct ink writing of ceramic matrix composite structures.* Journal of the American Ceramic Society, 2017. **100**(10): p. 4397-4401.
21. Niendorf, K. and B. Raeymaekers, *Additive manufacturing of polymer matrix composite materials with aligned or organized filler material: a review.* Advanced Engineering Materials, 2021. **23**(4): p. 2001002.
22. Rashid, A.B., et al., *Breaking Boundaries with Ceramic Matrix Composites: A Comprehensive Overview of Materials, Manufacturing Techniques, Transformative Applications, Recent Advancements, and Future Prospects.* Advances in Materials Science and Engineering, 2024. **2024**(1): p. 2112358.
23. Madhankumar, A. and A. Xavior, *Graphene reinforced ceramic matrix composite (GRCMC)–state of the art.* Engineering Research Express, 2024.
24. Krstić, V.D. *Ceramic matrix composites-present status and future trends*. in *Materials science forum*. 1998. Trans Tech Publ.
25. Saha, M. and M. Mallik, *Additive manufacturing of ceramics and cermets: present status and future perspectives.* Sādhanā, 2021. **46**(3): p. 162.
26. Tuersley, I., A. Jawaid, and I. Pashby, *Various methods of machining advanced ceramic materials.* Journal of Materials Processing Technology, 1994. **42**(4): p. 377-390.
27. Shrivastava, S., et al., *Ceramic Matrix Composites: Classifications, Manufacturing, Properties, and Applications.* Ceramics, 2024. **7**(2): p. 652-679.
28. O'Masta, M.R., et al., *Additive manufacturing of polymer-derived ceramic matrix composites.* Journal of the American Ceramic Society, 2020. **103**(12): p. 6712-6723.
29. Athanasiadis, M., et al., *Direct writing of elastic fibers with optical, electrical, and microfluidic functionality.* Advanced Materials Technologies, 2019. **4**(7): p. 1800659.
30. Wang, W., et al., *Additive manufacturing of fiber reinforced ceramic matrix composites: Advances, challenges, and prospects.* Ceramics International, 2022. **48**(14): p. 19542-19556.
31. Wei, P., et al., *Go with the flow: Rheological requirements for direct ink write printability.* Journal of Applied Physics, 2023. **134**(10).
32. Thiraux, R., et al., *Damage tolerance in additively manufactured ceramic architected materials.* Journal of the European Ceramic Society, 2022. **42**(13): p. 5893-5903.
33. Saadi, M., et al., *Direct ink writing: a 3D printing technology for diverse materials.* Advanced Materials, 2022. **34**(28): p. 2108855.
34. Center, U.H.E. *Hershel-Bulkley Parameters. Hershel-Bulkley parameters*. Available from: https://www.hec.usace.army.mil/confluence/rasdocs/rasmuddebris/non-newtonian-user-s-manual/user-inputs-and-model-parameters/hershel-bulkley-parameters#:~:text=The%20Herschel-Bulkley%20model%20simulates,material%20more%20difficult%20to%20deform
35. del-Mazo-Barbara, L. and M.-P. Ginebra, *Rheological characterisation of ceramic inks for 3D direct ink writing: A review.* Journal of the European Ceramic Society, 2021. **41**(16): p. 18-33.
36. Zhou, C., et al., *Preparation of 3D-Cf/SiC composites at low temperatures.* Materials Science and Engineering: A, 2008. **488**(1-2): p. 569-572.
37. Chai, Y., et al., *Effect of pyrolysis temperatures on the performance of SiCf/SiC*

composites. Fusion Engineering and Design, 2017. **125**: p. 447-453.
38. Lu, Z., et al., *Microstructure control of highly oriented short carbon fibres in SiC matrix composites fabricated by direct ink writing.* Ceramics International, 2019. **45**(14): p. 17262-17267.
39. Franchin, G., et al., *Optimization and characterization of preceramic inks for direct ink writing of ceramic matrix composite structures.* Materials, 2018. **11**(4): p. 515.
40. Xing, H., et al., *Fabrication and characterization of SiC whiskers toughened Al2O3 paste for stereolithography 3D printing applications.* Journal of Alloys and Compounds, 2020. **828**: p. 154347.
41. Liu, Y., et al., *Continuous carbon fiber reinforced ZrB2-SiC composites fabricated by direct ink writing combined with low-temperature hot-pressing.* Journal of the European Ceramic Society, 2022. **42**(9): p. 3699-3707.
42. Lu, Z., et al., *Manufacturing properties of turbine blades of carbon fiber-reinforced SiC composite based on stereolithography.* Materials and Manufacturing Processes, 2014. **29**(2): p. 201-209.
43. Zhang, H., et al., *Stereolithography-based additive manufacturing of lightweight and high-strength Cf/SiC ceramics.* Additive Manufacturing, 2020. **34**: p. 101199.
44. Zhang, H., et al., *The preparation of SiC-based ceramics by one novel strategy combined 3D printing technology and liquid silicon infiltration process.* Ceramics International, 2019. **45**(8): p. 10800-10804.
45. Xia, Y., et al., *Microstructure and mechanical property of Cf/SiC core/shell composite fabricated by direct ink writing.* Scripta Materialia, 2019. **165**: p. 84-88.
46. Mera, G., et al., *Ceramic nanocomposites from tailor-made preceramic polymers.* Nanomaterials, 2015. **5**(2): p. 468-540.
47. Mikolajek, M., et al., *Control of the surface morphology of ceramic/polymer composite inks for inkjet printing.* Advanced Engineering Materials, 2018. **20**(9): p. 1800318.
48. Hurwitz, F.I., *Ceramic matrix and resin matrix composites: A comparison*. 1987.
49. Davis, H. and D. Petrak, *Ceramic matrix composites using polymer pyrolysis and liquid densification processing.* Journal of nuclear materials, 1995. **219**: p. 26-30.
50. Apostolov, Z.D., et al., *Effects of low-temperature treatment on the properties of commercial preceramic polymers.* Journal of the European Ceramic Society, 2020. **40**(8): p. 2887-2895.
51. Diefendorf, R. and R. Boisvert, *Processing of polymeric precursor, Ceramic matrix composites.* MRS Online Proceedings Library, 1988. **120**: p. 157-162.
52. Samokhin, A. *Open-Source Syringe Pump*. 2020; Available from: https://www.mass-spec.ru/projects/diy/syringe_pump/eng/.
53. Vinci, A., et al., *Oxidation behaviour of a continuous carbon fibre reinforced ZrB2–SiC composite.* Corrosion Science, 2017. **123**: p. 129-138.
54. Wang, Q., et al., *Development of a carbonization-in-nitrogen method for measuring the fiber content of carbon fiber reinforced thermoset composites.* Composites Part A: Applied Science and Manufacturing, 2015. **73**: p. 80-84.
55. Magnant, J., et al., *Carbon fiber/reaction-bonded carbide matrix for composite materials–manufacture and characterization.* Journal of the European Ceramic Society, 2012. **32**(16): p. 4497-4505.
56. Jin, W., et al., *Oxidation behavior and high-temperature flexural property of CVD-SiC-*

coated PIP-C/SiC composites. Ceramics International, 2018. **44**(14): p. 16583-16588.